

## Star Formation in the Rosette Complex

Carlos G. Román-Zúñiga

*Centro Astronómico Hispano Alemán,  
Jesús Durbán Remón 2-2, Almería 04004, Spain*

Elizabeth A. Lada

*Astronomy Department, University of Florida,  
211 Bryant Space Sciences Center, Gainesville, FL 32611, USA*

**Abstract.** The Rosette Complex in the constellation of Monoceros is a magnificent laboratory for the study of star formation. The region presents an interesting scenario, in which an expanding HII region generated by the large OB association NGC 2244 is interacting with a giant molecular cloud. Inside the cloud a number of stellar clusters have formed recently. In this chapter we present a review of past and present research on the region, and discuss investigations relevant to the physics of the nebula and the molecular cloud. We also review recent work on the younger embedded clusters and individual nebulous objects located across this important star forming region.

### 1. Historical Perspective

The Rosette Complex ( $l = 207.0$ ,  $b = -2.1$ ) is located near the anti-center of the Galactic Disk in the constellation of Monoceros. The region is very popular, partly because of the staggering beauty of its main feature: a very extended emission nebula which hosts a large central HII region, evacuated by the winds of a central OB association (see Figure 1).

The complex is part of a much larger structure known as the Northern Monoceros Region. This region comprises the Mon OB1 Cloud (host of NGC 2264 and the Cone Nebula), the Monoceros Loop (NGC 2252), and the Mon OB2 Cloud in which the Rosette is one of the most prominent features (see Figure 2).

The catalog name for the Rosette can be somewhat confusing because it is not unique: The nebula itself is usually cataloged as NGC 2237 or NGC 2246 (especially by amateur observers), although NGC 2237 originally referred to the brightest patch at its western side and NGC 2246 originally pointed to a bright zone at the eastern side. In addition, while the central cluster is usually known as NGC 2244, it has also been cataloged as NGC 2239. However, this latter designation historically referred to the brightest star in the region, 12 Monocerotis.

The cluster was first noticed by Flamsteed in the late 17th century and later reported by William Herschel — who did not notice the nebulosity — and John Herschel, who discovered several conspicuous nebulosity features and reported them in his general catalog (Herschel 1864, NGC 2239 = GC 1420). A contemporary report on nebulous emission was done by Albert Marth (Lassell 1867, NGC 2238 = GC 5361 = Marth 99), who described a “small, faint star in nebulosity.”

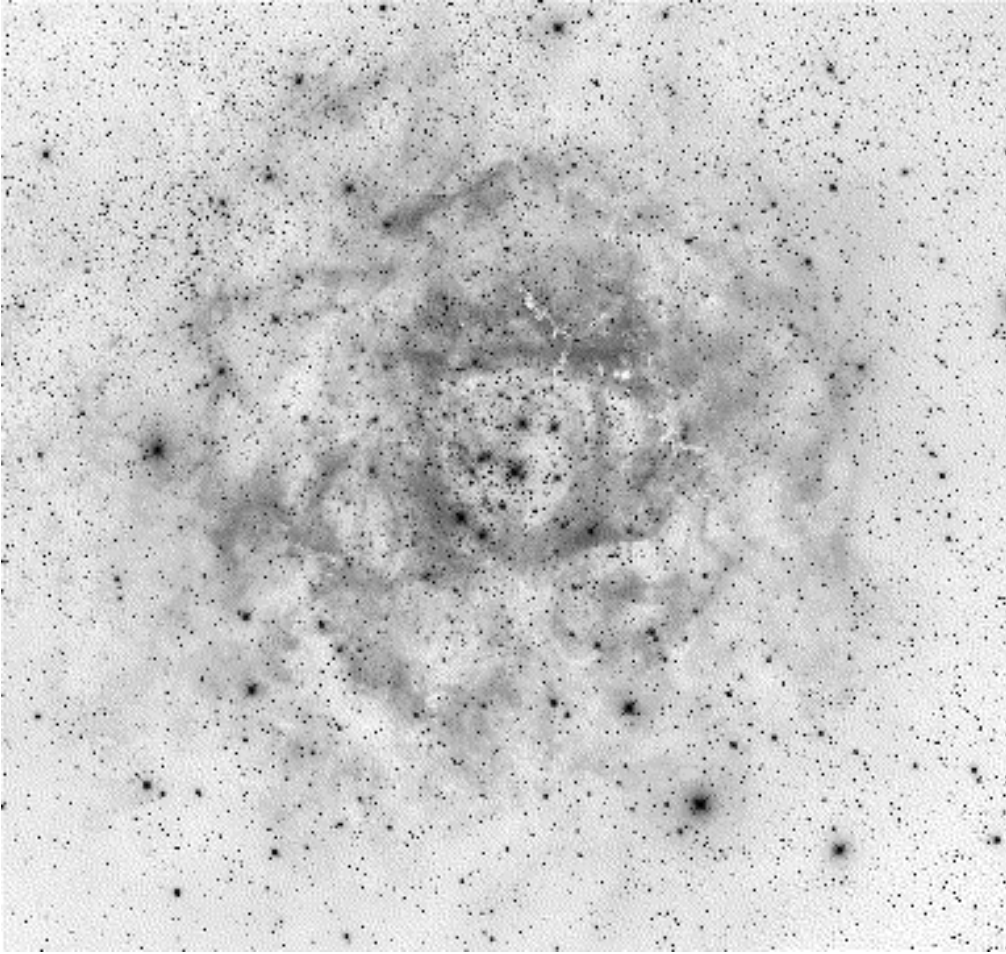


Figure 1. The majestic Rosette Nebula in Monoceros. Image courtesy of Robert Gendler.

Other parts of the nebula (NGC 2237 and NGC 2246) were reported by Swift (1885) who cataloged the object as being “pretty bright [pB], very, very large [vvL] and diffuse [diff].” Afterwards, the region was formally known as the “Swift Nebula,” until the name “Rosette” became more popular. The total extent of the Rosette was not determined until the first photographic plates were obtained by Barnard (1894).

Two of the first applications of Rosette Nebula photographic data were made by Hubble (1922) in his study of diffuse nebulae associated with massive stars, and Minkowski (1949), who published a photographic study along with a first discussion on the expansion of the HII region by the winds of O stars in the central cluster. Minkowski also pointed out the existence of elephant trunks and dark globules. He estimated the mass of the nebula to be  $10^4 M_{\odot}$  and suggested that it could be “surrounded and probably embedded in obscuring material,” thus proposing the existence of the companion molecular cloud.

The first formal radio wavelength observation of the Rosette Nebula was reported by Ko & Kraus (1955). They surveyed the area with the Ohio State University antenna

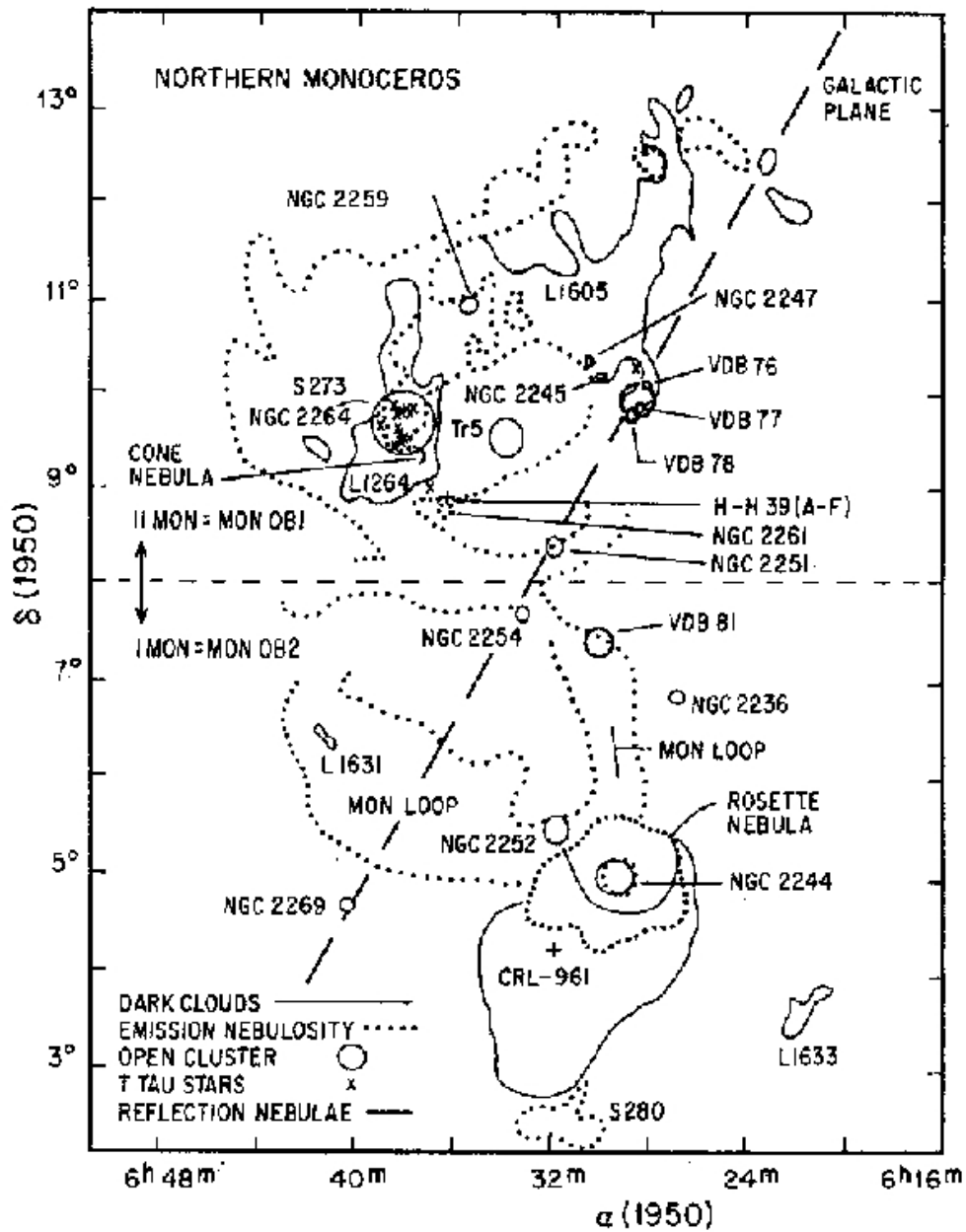


Figure 2. The location of the Rosette in the context of the Monoceros Complex, from Pérez (1991)

at 187.5 MHz with a HPBW resolution of  $1.3'$ , and calculated a blackbody temperature of 200 K for the nebula. Later, Menon (1962) used the 85 ft. Tatel telescope to make a very complete study of the nebula at 3 GHz (10 cm). His analysis showed convincingly that the Rosette Nebula is an ionization bounded Strömgren sphere and he discussed

how it could have formed from a fraction of a large dark cloud with a total mass of approximately  $1.4 \times 10^4 M_{\odot}$ .

## 2. The Rosette Nebula and the Young Cluster NGC 2244

### 2.1. The Rosette Nebula

Ogura & Ishida (1981) tabulated the different methods used to determine the age of the nebula. These varied from studies of the properties of the central cavity (Kahn & Menon 1961; Lasker 1966) to evolutionary models of the HII region based on the luminosity of the stars (Hjellming 1968). Other methods involve time scales of radiation pressure (Mathews 1966, 1967), estimates of the formation time for dark globules in the nebula (Herbig 1974), and the separation of [OIII] emission lines (Smith 1973). The median value of all these age estimates is approximately  $3 \pm 1 \times 10^6$  yr.

A series of studies by Celnik (1983, 1985, 1986) discussed the global physical characteristics of the Rosette Complex. The first two of these are dedicated to the nebula, while the third one is a model of the interaction with the molecular cloud, thus we defer its discussion to Section 3. In the first of the Celnik articles, he presented a map of the  $H\alpha$  emission in the nebula region, and calculated a total integrated flux density of  $5 \times 10^{-11} \text{ W}\cdot\text{m}^{-2}$  within  $60'$  from the center of the HII cavity. He suggested that the emission is contained in a more or less symmetric ring with a peak at  $16'$  from the center.

Table 1. Distance Estimates to the Rosette (NGC 2244)

Author	Value (pc)	Method
Johnson (1962)	1660	Photoelectric Photometry
Ogura & Ishida (1981)	1420	Visual Photometry
Pérez et al. (1987)	1670	Visual Photometry
Park & Sung (2002)	1660	Visual Photometry
Hensberge et al. (2002)	1390	Spectroscopy

In the second paper, Celnik reported radio continuum observations (1410 and 4750 MHz) from which he was able to determine that the nebula is bound by ionization, forming a spherical shell with radius of  $\sim 20$ -30 pc (in agreement with the 3.7, 7.7 and 14.3 GHz observations of Kaidanovskii 1980) and a total ionized matter mass of  $2.3 \times 10^4 M_{\odot}$  (almost twice the estimate of  $1.1 \times 10^4 M_{\odot}$  by Menon 1962). Using the  $H112\alpha$  and  $He112\alpha$  (4619 and 4621 Mhz) radio recombination lines (RRL) Celnik calculated a  $He^+$  abundance of  $0.12 \pm 0.03$  and a non-LTE average electron temperature for the nebula of  $T_e = 5800 \pm 700$  K — almost 1100 K above the LTE — with no evidence for a significant gradient with respect to the radial distance from the center.

However, other studies revealed that the LTE temperature of the Rosette was definitely not uniform. For example Pedlar & Matthews (1973) found  $T_e$  values between  $6400 \pm 1300$  and  $8160 \pm 1100$  K (average of 7900 K) across the nebula using  $H166\alpha$  RRL (1424 MHz). In a similar study, Viner et al. (1979) calculated non-LTE values between  $3900 \pm 700$  and  $6000 \pm 500$  K from  $H100\alpha$  RRL (6480 MHz) observations. The 25 MHz observations (decameter length) of Krymkin (1978) suggested a median  $T_e$  of 3600 K. Later, Deshpande et al. (1984) using continuum absorption observations at

34.5 MHz combined with 2700 MHz observations by Graham et al. (1982) argued that the electron temperature might vary from approximately 5000 K in the southeastern quadrant of the nebula — which contains more dust from the interface with the molecular cloud — to roughly 8000 K at the northwestern regions. Finally, Tsivilev et al. (2002) presented observations of the H $92\alpha$  RRL at three points coincident with crucial positions of the 4750 MHz map of Celnik which revealed a higher average temperature of  $7980\pm 580$  K. They also discussed all other RRL measurements of the Rosette Nebula available in the literature, and found  $T_e$  measurements to vary from 3000 to 10050 K.

The investigation by Shipman & Clark (1994) revealed a good fit to a  $T \propto r^{-\alpha}$ ,  $\alpha = 0.4$  model for the temperature gradient in the nebula cavity which, interestingly, could not be adjusted to the observed IRAS emission. Instead, they found that this temperature gradient was better adjusted to  $\alpha = 0.05$  for  $r < 47'$  and  $\alpha = 0.2$  for  $47' < r < 65'$  (see also Section 3.2).

The pioneering observations by Gosachinskii & Khersonskii (1982) of the HI emission at 21 cm made with the RATAN-600 telescope revealed that the Rosette Complex and the Monoceros Loop were enclosed in a thin HI envelope 130 pc in diameter, possibly expanding at  $20 \text{ km}\cdot\text{s}^{-1}$ , suggesting that the supernova event that gave origin to the Monoceros remnant occurred about  $1.8 \times 10^4$  yr ago. The study of Guseva et al. (1984) discussed in detail how the supernova event in Monoceros could in fact be responsible for the collision of clouds that triggered star formation in NGC 2264 (1 Mon) and the Rosette Complex (2 Mon). Later, Kuchar & Bania (1993) made a new, local 21 cm map of the Rosette Complex using the Arecibo telescope. They found that neutral gas in the Rosette Complex is distributed in three main regions which form a rough, extended shell of about 45 pc in radius around the nebula and extend beyond the molecular cloud. This shell would have a center of expansion at  $(\alpha, \delta) = (6^h 31^m 48^s, 4^d 59' 12'')$ , J2000, and has a mass close to  $2 \times 10^4 M_{\odot}$ , which implies a budget of kinetic energy for the shell expansion of approx.  $4 \times 10^{48}$  ergs, or roughly 2% of the total energy available from the stars in NGC 2244.

## 2.2. NGC 2244

The prominent OB association NGC 2244 contains more than 70 high mass sources with spectral types O and B (7 and 24 sources respectively, see Table 2). The stars in the cluster are presumed responsible for the evacuation of the central part of the nebula. Flynn (1965) used a Fabry-Perot interferometer to study the velocity distribution of the low density gas in the cavity and its relation to the cluster. A subsequent analysis by Smith (1968) suggested an initial streaming velocity of  $13 \text{ km}\cdot\text{s}^{-1}$  at the ionization front. Later, in the study of Fountain et al. (1979), 700 positions in the nebula were analyzed with multi-slit echelle spectroscopy in H $\alpha$ , and these data revealed large systematic velocities of up to  $20 \text{ km}\cdot\text{s}^{-1}$  at the cavity, a sign of rapid evacuation of material due to powerful stellar winds. A similar result was found by Smith (1973).

The cluster itself has been the subject of many detailed studies over the years. The distance to this young cluster (and therefore to the entire complex) has been estimated many times with slightly different results. Table 1 is a compilation of these values, from which the most commonly used is 1600 to 1700 pc.

*Optical Studies* Some of the first visual photometric studies of NGC 2244 were made by Kirillova (1958), who constructed the first HR diagram of the cluster and assigned

to it a distance modulus of 12.1 mag, and by Johnson (1962), who estimated the mean color excess in the cluster to be  $E(B - V) = 0.46$  for  $R = A_V/E(B - V) = 3.0$ . This was confirmed by Turner (1976) and later Ogura & Ishida (1981), who suggested a value of  $R = 3.2 \pm 0.15$ . Ogura & Ishida (1981) also proposed an age of  $4 \pm 1$  Myr and a star formation efficiency of 22% for the cluster. Later, Marschall et al. (1982) completed a proper motion study of 287 stars in the NGC 2244 area. They confirmed membership for 113 objects, 52 of them from the list of Ogura & Ishida (1981).

A study that combined photometry as well as spectroscopy was completed by Pérez et al. (1987). They found that some members of NGC 2244 presented anomalous values of  $R$ , possibly suggesting the coexistence of main sequence stars with very young objects—likely T Tauri stars. This was confirmed in the  $uvby\beta$  photometry study (Pérez et al. 1989), in which 4 members presented evidence of being true pre-main sequence (PMS) objects. Pérez et al. (1989) also confirmed the age of NGC 2244 to be below 4 Myr but spread towards younger values, thus confirming a model of continuous formation.

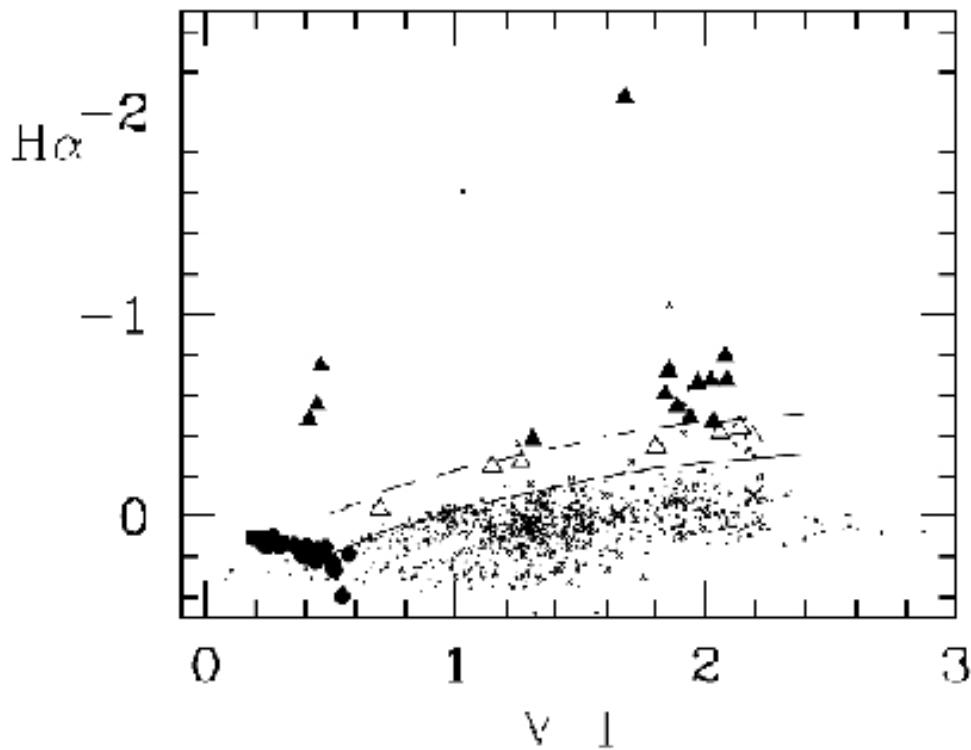


Figure 3. An  $H\alpha$  vs.  $V-I$  diagram for NGC 2244. The solid line represents a ZAMS relation while the dashed line is a selection limit. Filled triangles are PMS stars while open triangles are PMS candidates. Bright members are marked with dark filled circles. X symbols are X-ray sources and dots are non-members. From Park & Sung (2002).

A study of great importance was performed by Park & Sung (2002). They obtained UBVI and  $H\alpha$  photometry for the cluster. They were able to determine member-

ship for a total of 30 cluster sources and to extend the list of known PMS candidates to 21. They subsequently identified members coincident with ROSAT point source catalogs and compared their properties to the rest of the sample. Six of the PMS candidates were confirmed as X-ray sources. In Figure 3, we show the Park & Sung diagram of  $H\alpha$  emission vs. V-I color for NGC 2244. In this figure, PMS stars are clearly located above the main sequence.

Using evolutionary models, Park & Sung showed that most of the PMS stars and PMS candidates in their sample appear to have masses close to  $1 M_{\odot}$  and an approximate mean age of 0.4 to 0.9 Myr. Later, they estimated the main sequence turn-off age of the cluster to be 1.9 Myr, thus suggesting that the cluster has not stopped forming stars yet.

Another important determination by Park & Sung is the Initial Mass Function (IMF) of NGC 2244. They found it has a flat ( $\Gamma = -0.7$ ) IMF slope in the range  $0.5 \leq \log m \leq 2.0$ , which compares well with the  $\Gamma = -0.8$  slope obtained by Massey et al. (1995). By comparing directly to the IMF model of Scalo (1986) and to the observed mass function of NGC 2264, Park & Sung suggested that the shape of the stellar mass spectrum of NGC 2244 was dominated by high mass stars. However, they cautioned about the lack of sensitivity at the intermediate and low mass ranges in their sample. More recently, Wang et al. (2008), showed that NGC 2244 actually has a standard IMF shape regardless of the large number of massive stars.

*Spectroscopic Studies* The most complete spectroscopic study of NGC 2244 was done by Verschueren (1991), and it has been widely used in the literature. In particular, Park & Sung used Verschueren (1991) data to identify the spectral types of candidate T Tauri stars in NGC 2244. Most of available spectral classifications for stars in NGC 2244 are compiled by Ogura & Ishida (1981), but additional data can be found in Pérez et al. (1987) and Massey et al. (1995) (see also Chen et al., 2004 and references therein).

A low resolution, single slit investigation by Hensberge et al. (1998) of 2 members and 3 field stars in the region of NGC 2244 yielded evidence that these were chemically peculiar, possibly magnetic stars. Hensberge et al. (2000) performed spectroscopic analysis of the binary member V578 Mon, which resulted in an estimated distance slightly lower than other photometric estimates (see Table 1). They also calculated the age of the system to be  $2.3 \pm 0.2$  Myr. Another study by Bagnulo et al. (2004) revealed that the source NGC2244-334 (a He-weak B5 V type star) has a very large longitudinal magnetic field ( $-9$  kG), which is the second largest found in a non-degenerate star. They suggest that given the age of NGC 2244, this source might also be among the youngest Ap-Bp stars ever observed, suggesting that these kind of sources can show magnetic fields from their birth. Li et al. (2002) presented low resolution spectra for a sample of X-ray counterparts from the ROSAT PSPC survey (see also Gregorio-Hetem et al. 1998). They were able to confirm that five sources had strong  $H\alpha$  emission. Two of the stars were found to be Herbig Ae/Be and two others appear to be WTTS. These data indicate that X-rays are an efficient tracer of young populations.

*Near Infrared* Recent surveys in the near-infrared have permitted investigation of the extension and structure of NGC 2244. Li (2005) analyzed 2MASS data and suggested that NGC 2244 had a second component located approximately 6.6 pc west of the core center. Data from the FLAMINGOS Survey (Román-Zúñiga et al. 2008) confirmed the existence of this second association, which is coincident with the area originally

Table 2. OB Members of the Young Cluster NGC 2244

Star ID <sup>a</sup>	RA <sup>b</sup> DEC <sup>b</sup>		Sp. Type <sup>c</sup>	V <sup>d</sup> K		Other <sup>e</sup>
	J2000			[mag]		
HD 46223	06 32 09.32	+04 49 24.6	O4V((f))	7.32	6.68	OI81-203
HD 46150	06 31 55.52	+04 56 34.3	O5V((f))	6.75	6.44	OI81-122
HD 46485	06 33 50.95	+04 31 31.6	O7V	8.20	7.45	OI81-387
HD 46056	06 31 20.87	+04 50 03.9	O8V((f))	8.16	7.82	OI81-84
HD 46149	06 31 52.54	+05 01 59.1	O8.5V((f))	7.59	7.25	PS-160
HD 258691	06 30 33.31	+04 41 27.6	O9V((f))	9.70	7.93	OI81-376
HD 46202	06 32 10.48	+04 57 59.7	O9V((f))	8.20	7.72	PS-305
HD 259238	06 32 18.22	+05 03 21.7	B0V	11.10	10.28	PS-348
HD 46106	06 31 38.40	+05 01 36.3	B0.2V	7.95	7.62	PS-75; OI81-115
MJD95	06 31 37.08	+04 45 53.7	B0.5V	15.15	12.20	—
HD 259135	06 32 00.61	+04 52 41.0	B0.5V	8.54	8.12	PS-226; OI81-200
GSC 00154-00234	06 33 37.49	+04 48 47.0	B0.5V	11.89	8.64	—
HD 259012	06 31 33.46	+04 50 39.7	B1V	9.35	8.79	PS-43; OI81-80
HD 259105	06 31 52.00	+04 55 57.3	B1V	9.42	8.95	PS-155; OI81-128
GSC 00154-02337	06 32 06.13	+04 52 15.3	B1III	9.73	9.39	PS-269; OI81-201
HD 46484	06 33 54.41	+04 39 44.6	B1V	7.65	6.87	OI81-389
BD+05 1281B	06 31 58.93	+04 55 39.9	B1.5V	10.38	9.74	PS-214; OI81-193
HD 259172	06 32 02.59	+05 05 08.6	B2V	10.71	10.09	PS-240; OI81-167
GSC 00154-02247	06 33 06.56	+05 06 03.4	B2	12.85	11.20	OI81-345
GSC 00154-02504	06 31 31.47	+04 50 59.6	B2.5V	10.64	10.24	PS-34; OI81-79
GSC 00154-02141	06 31 47.89	+04 54 18.1	B2.5V	11.66	10.87	PS-123; OI81-130
GSC 00154-02187	06 31 58.91	+04 56 16.2	B2.5Vn	11.26	10.54	PS-213; OI81-190
GSC 00154-01007	06 32 09.84	+05 02 13.4	B2.5V	11.22	10.43	PS-300; OI81-172
GSC 00154-01016	06 32 24.24	+04 47 03.7	B2.5V	11.41	10.58	PS-398; OI81-274
GSC 00154-01247	06 33 50.56	+05 01 37.6	B2.5V	11.12	9.99	OI81-392
GSC 00154-01753	06 32 15.49	+04 55 20.4	B3	12.01	10.96	PS-327; OI81-194
MJD95	06 32 22.49	+04 55 34.2	B3V	15.39	13.48	PS-383
HD 259268	06 32 23.04	+05 02 45.7	B3	11.09	10.33	PS-390
HD 259300	06 32 29.39	+04 56 56.1	B3Vp	10.79	9.34	PS-441
MJD95	06 33 10.16	+04 59 49.9	B3V	14.98	12.39	—
GSC 00154-02164	06 32 51.79	+04 47 16.2	B5V	12.88	11.53	OI81-334

<sup>a</sup> Star identification. HD catalog is used when available, followed in priority by GSC and BD catalogs. Stars listed as MJD95 are identified by position in the list of Massey et al. (1995).

<sup>b</sup> Coordinates from the 2MASS Point Source Catalog

<sup>c</sup> Spectral types as listed by Wang et al. (2008), except GSC 00154-02164

<sup>d</sup> Visual (V) photometry from Ogura & Ishida (1981), Massey et al (1995) and Park & Sung (2002). Near-infrared (K) photometry from the 2MASS Point Source Catalog.

<sup>e</sup> Correspondence with the lists of Ogura & Ishida (1981) [OI] and Park & Sung (2002) [PS].

labeled as NGC 2237. In Figure 4 we show the locations of infrared excess (IRX) sources with local surface densities above the field levels. The extinction in the region is rather low ( $\langle A_V \rangle \approx 3.0$ ) compared to the molecular cloud areas but the distribution of excess sources is well defined and trace the location and extension of NGC 2244 and the satellite cluster.

Using a cross-referenced catalog of NGC 2244 (Román-Zúniga & Lada, in preparation) which includes data from the 2MASS and FLAMINGOS near-infrared surveys and the survey of Park & Sung (2002), we were able to construct two optical-infrared photometric diagrams: Figure 5 is an optical-infrared color-magnitude dia-



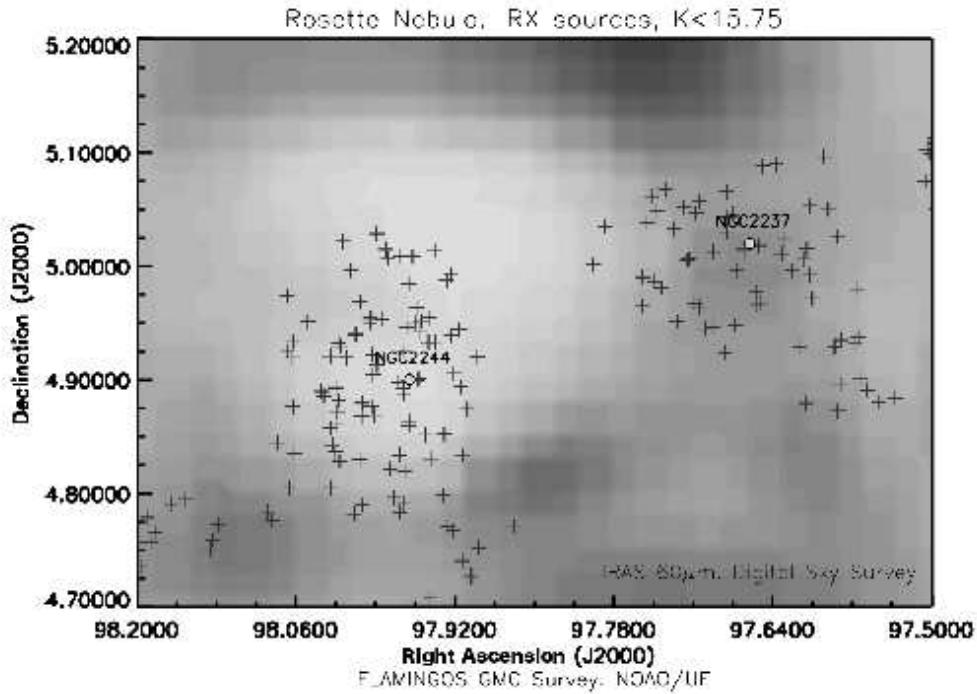


Figure 4. Infrared Excess sources with significant local surface densities in the central part of the Rosette Nebula, from the FLAMINGOS survey. The clusters NGC 2244 and a possible companion cluster at the west region of the nebula, NGC 2237, are traced by this population. The background levels indicate  $60 \mu\text{m}$  emission from IRAS, in steps of  $5.0 \text{ Jy}$ . Adapted from Román-Zúñiga et al. (2008).

gram in which probable members ( $P=0.6$  or more) from the study of Marschall et al. (1982) are shown with dark symbols. The 1,2,3 and 5 Myr isochrones from the pre-main sequence evolutionary models of D’Antona & Mazzitelli (1997) are also shown. The 1-3 Myr isochrones are in good agreement with our data (at least for those stars which are less affected by reddening). Notice that the D’Antona & Mazzitelli models are calculated only for stars with  $3 M_{\odot}$  or less.

Figure 6 is an infrared color-color diagram of NGC 2244. The scarcity of sources along the reddening band shows that the extinction towards NGC 2244 is rather low, as the parental material has been almost completely evacuated. A few of the compiled stars have large H-K colors and are located to the right of the reddening band with similar slope and direction as the classical T Tauri locus (Meyer et al. 1997), but with slightly bluer J-H colors likely caused by nebular gas extinction (Héraudeau et al. 1996; Ishii et al. 2002). Another interesting feature is that some of the cluster members (solid symbols) form a locus that protrudes to the right of the reddening band, coincident with the observed locus for Be stars (Howells et al. 2001; Subramaniam et al. 2005), which suggests the presence of circumstellar material around some of the massive members of the association.

In Table 2 we present a list of the O and B members of NGC 2244, as listed in the X-ray studies by Townsley et al. (2003) and Wang et al. (2007). The list includes

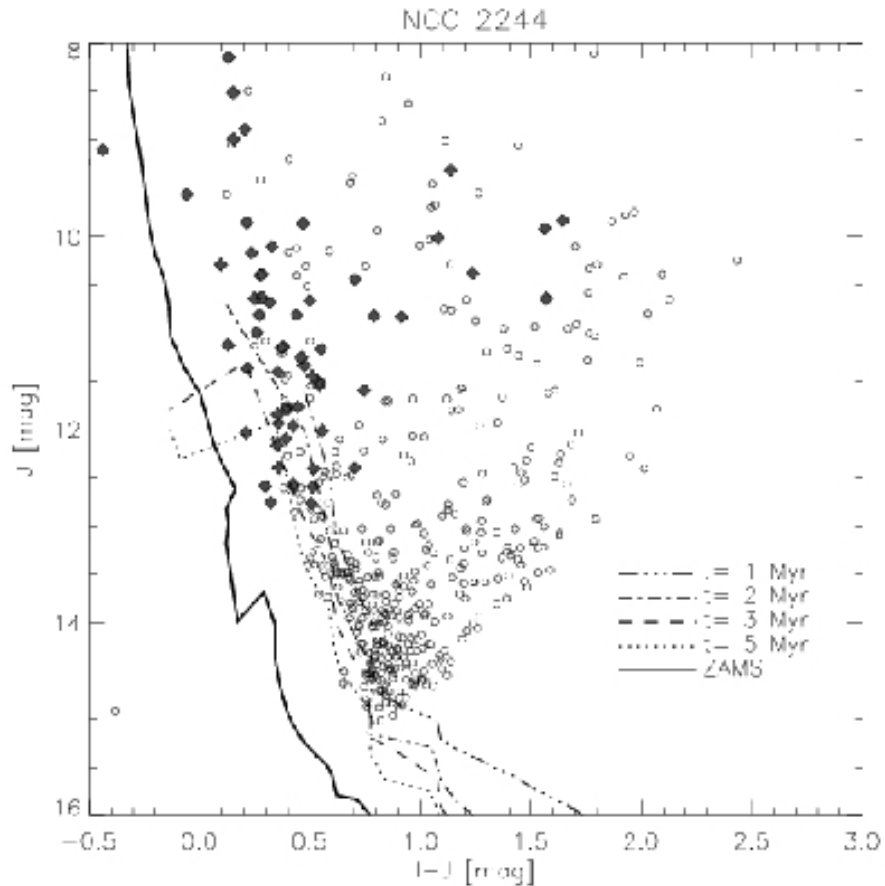


Figure 5. An optical-infrared color-magnitude diagram for NGC 2244. The solid diamond symbols have membership probabilities higher than 60%. The broken lines are model PMS isochrones at 1, 2, 3 and 5 Myr from D’Antona and Mazzitelli (1997). The thick solid line is the ZAMS.

identifications, positions, spectral types, B and K photometry and a cross identification with the lists of Ogura & Ishida (1981) and Park & Sung (2002).

*Mid-Infrared Observations* NGC 2244 was observed with the Infrared Array Camera (IRAC) and the Multiband Imaging Photometer (MIPS) on board the Spitzer Space Telescope in 2004 and 2005, respectively. Balog et al. (2007) obtained from these observations a catalog with more than a thousand high quality sources detected simultaneously at the four IRAC bands (3.6, 4.5, 5.8 and 8.0  $\mu\text{m}$ ), plus a total of 279 MIPS counterparts at 24  $\mu\text{m}$ , succeeding in completing a census of NGC 2244 in the mid-infrared down to a mass limit of  $\sim 0.8 M_{\odot}$ . The main purpose of the study of Balog et al. was the investigation of circumstellar disk survival in the OB environment.

A total of 337 and 25 sources were successfully identified as Class II and Class I sources, respectively (with 213 and 20 sources identified likewise in the IRAC-MIPS

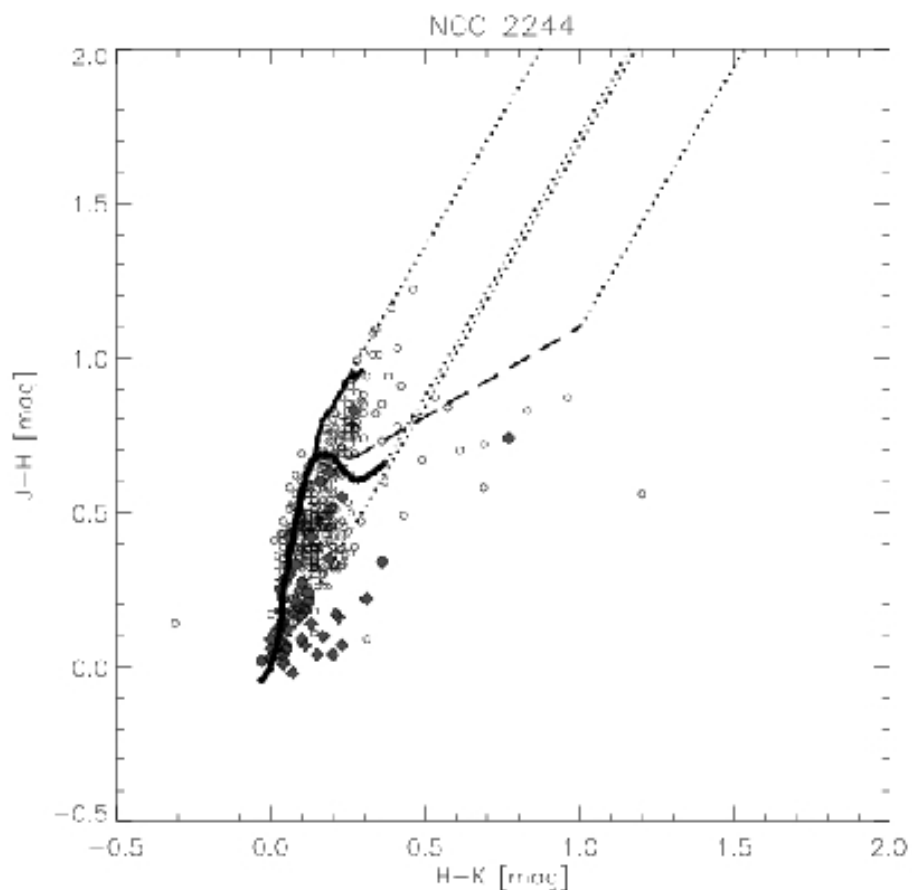


Figure 6. A near-infrared color-color diagram of NGC 2244. The solid diamond symbols have membership probabilities higher than 60%. The solid black lines indicate the ZAMS for dwarfs and giants, while the dotted lines indicate the reddening band from the law of Cohen (1981).

combined catalog). This implies that the ratio of Class I to Class II sources in NGC 2244 is less than 7%, much lower than the ratios observed in star forming regions with smaller proportions of massive stars. Balog et al. found that Class I sources are preferentially located at the outer regions of the cluster, with none located near the central parsec, opposite from the Class II sources which appear to concentrate around the OB center. These two aspects suggest that within the cluster star formation might have stopped, but it continues outside the HII region (see Figure 7).

Later, Balog et al. divided the detections into stars with and without infrared excess to give an estimate of the disk ratio in the cluster. They found that the disk ratio within 0.5 pc from the center of the cluster is 27%, then it increases to about 45% within 0.5 and 2.5 pc. The average disk fraction is thus above 40%, in close agreement with Haisch et al. (2001) which suggest that the disk fraction in a cluster decreases from 80

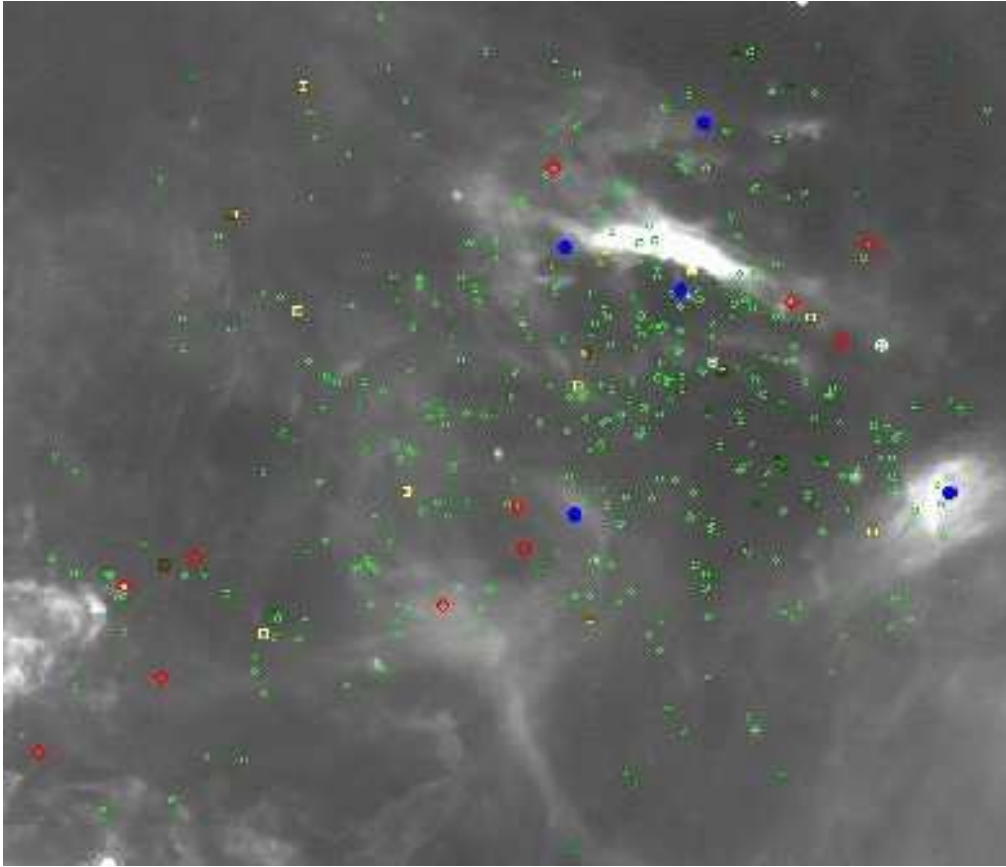


Figure 7. Distribution of candidate Class I sources (diamonds), Class II sources (circles), Class I-II sources (squares) and O stars (solid circles) in NGC 2244, overlaid on a  $24\ \mu\text{m}$  image obtained with MIPS onboard the Spitzer Space Telescope. Adapted from Balog et al. (2007).

to 50% within the first 2-3 Myr of life of a cluster<sup>1</sup>. The disk fraction in NGC 2244 calculated by Balog et al. is not very different ( $\Delta \approx 10\%$ ) from those found in clusters of similar age without O stars, plus they found a steep decrease of the photoevaporation rate as a function of distance from the cluster center, allowing them to conclude that the effect of high mass stars on disks is only significant at very close distances to the hot stars.

*X-Ray Studies* NGC 2244 is an important target for X-ray studies due to the interest in investigating the nature of massive stars as sources of high energy photons. Observations made with the Einstein space telescope by Leahy (1985) revealed that the OB stars in NGC 2244 were embedded in a bubble of hot, low-density gas with diffuse X-ray emission at a temperature of 1 keV, possibly originated by hot shocks in

---

<sup>1</sup>For comparison, the disk fraction observed in the near-infrared is 12% (see Section 4.1), but such discrepancy is due to the fact that IRAC is more successful at detecting circumstellar material because the cold and hot dust that comprises circumstellar disks emits preferentially within 3 and  $10\ \mu\text{m}$

the stellar winds of O stars. The ROSAT Consortium observations (2000) yielded 34 X-ray sources in NGC 2244, with typical X-ray luminosities of  $10^{30} - 10^{32}$  ergs  $s^{-1}$ . Six of these X-ray sources are PMS candidates as reported by Park & Sung (2002). Berghöfer & Christian (2002) also studied NGC 2244 ROSAT sources and found that objects with the faintest X-ray emission have very high X-ray to optical luminosity ratios. They noted that the number of X-ray emitters associated with  $H\alpha$  emission in NGC 2244 is remarkable.

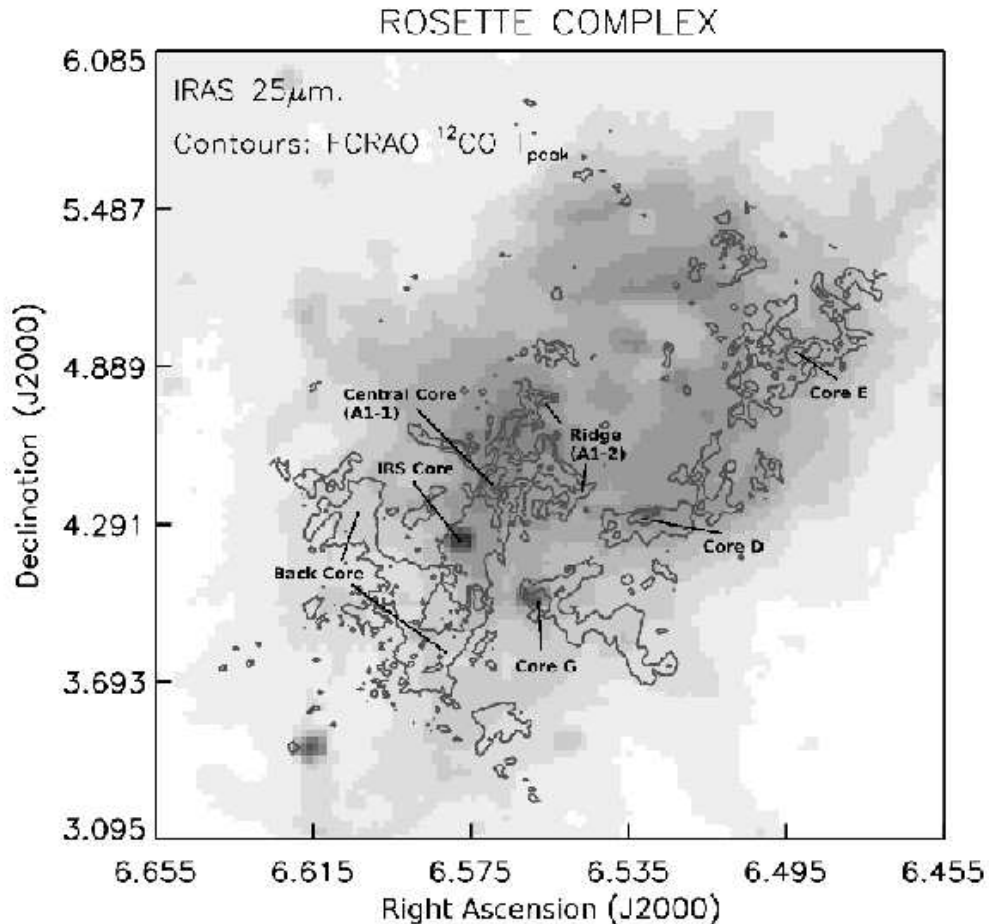


Figure 8. A map of the Rosette Complex. The background image is a plate of the IRAS survey at  $25 \mu\text{m}$ . The contours represent  $^{12}\text{CO}$  levels (as  $T_{peak}$ ) from the survey of Heyer, Williams, & Brunt (2006). Labels indicate the main regions of the molecular complex, originally identified by Blitz & Thaddeus (1980).

A more recent study by Chen et al. (2004) was dedicated also to analyze the coincidence of ROSAT with stars of NGC 2244. A careful re-sampling of the ROSAT data combined with new optical imaging and spectroscopic data yield 47 X-ray peaks with stellar counterparts in the Nebula region. Although it was estimated that about half of the counterparts were late type foreground stars, they could confirmed X-ray emission for the rest. Specifically, X-ray emission was confirmed for the 2 earliest type stars in the cluster (HD 46223 and HD 46150 with types O5 and O4 respectively), for

a very young binary (J063148.30+045820.5), for the source HD 259210 which coincides with the location of high speed knots identified by Meaburn & Walsh (1986), and for the source J063309.61+044624.5 located near a massive nebular pillar identified by Schneps et al. (1980) (see also Section 5.2). Taken together, all these investigations give strength to the hypothesis that X-ray emitters in NGC 2244 are either very massive or very young in the case of late types.

Probably the most sensitive X-ray observations of NGC 2244 to date were obtained with the Advanced CCD Imaging Spectrometer (ACIS) on board the Chandra space Observatory. The point source analysis by Wang et al. (2008) is complementary to the study of Townsley et al. (2003) which was dedicated to investigate the diffuse emission in the HII region (see Section 3.2). Within the ACIS mosaic, Wang et al. were able to extract, with high reliability, over 800 X-ray point sources within 20 arcmin from  $(\alpha, \delta) = (6^h 31^m 59^s, +4^d 55' 36'')$ , J2000). The X-ray sources have luminosities between  $10^{29.4}$  and  $10^{32.0}$  ergs·s<sup>-1</sup> in the hard band (2-8 keV). All sources with spectral types earlier than B1 were detected.

A total of 712 Chandra sources in the Wang et al. survey were found to be counterparts of near-infrared sources detected in the FLAMINGOS (see Section 4) and 2MASS surveys, down to a mass limit close to  $0.1 M_{\odot}$ . Among this X-ray selected sample, the fraction of stars with mass  $> 0.5 M_{\odot}$  with significant K-band excess (likely indicative of a circumstellar disk) is about 6%, and three of the sources were positively identified as potential Class I sources. The unobscured population in NGC 2244 is about 1.2 times larger than that of the ONC (Feigelson et al. 2005) and both the XLF and the KLF (constructed from the uniformly sampled 2MASS catalog) appears to suggest a normal Salpeter IMF for stars with mass  $> 0.5 M_{\odot}$ . By comparing to the ONC distribution, they estimate that the total population of NGC 2244 could be around 2000 members. The radial source density profile of X-ray sources appears to have a relaxed structure around the center of the cluster and suggests a low probability of significant mass segregation.

### 3. The Rosette Molecular Cloud and Embedded Populations

#### 3.1. Structure of the Rosette Molecular Cloud: CO studies

First attempts to detect CO emission associated with the Rosette nebula were unsuccessful as they pointed at the nebula region, which is mostly composed of neutral and ionized gas. The observations reported by Blitz & Thaddeus (1980), which targeted the southeast adjacent region of the nebula, were the first successful detections of molecular gas in the Rosette. Their NRAO survey mapped over 80% of the <sup>12</sup>CO emission in the area of the cloud with a 1' beam size, and yielded information about its large scale distribution. They estimated the angular extent of the cloud to be 3.5° (98 pc at a distance of 1600 pc) and labeled the most prominent sub-structures (see Figure 8).

Particularly important regions are the *Monoceros Ridge* (region A1-2) which is literally a region of gas compression at the cloud-nebula interface; the *central core* (A1-1), which hosts the most massive clumps in the cloud and is the strongest region of star formation; the cores D and G, which are separated from the main body of the cloud but have ongoing star cluster formation; the *IRS core*, which hosts the massive proto-binary AFGL-961 (see Sections 4 and 5.1); the *back core* B, which is more loose in structure than the regions near the nebula; and the *arm* or E core, which despite

its brightness contains no significant star formation (no IRAS sources, or near-infrared clusters have been found in this core so far).

In a subsequent study, Blitz & Stark (1986) mapped the  $^{12}\text{CO}$  and  $^{13}\text{CO}$  emission with improved sensitivity at the AT&T Bell Labs, uncovering the high degree of clumpiness of the cloud. Williams, de Geus, & Blitz (1994) made use of the data from Blitz & Stark and listed a total of 95 clumps. The clumps with evidence of star formation had larger peak temperatures, larger densities and also were more gravitationally bound compared to clumps from the Maddalena Complex (Maddalena & Thaddeus 1985), a cloud with very low star formation. Later, Williams et al. (1995) showed that about half of the clumps in the Rosette Molecular Cloud were gravitationally bound and the rest were supported by pressure from the inter-clump medium, which was shown to be mostly atomic and about 40 times less dense. In Figure 9 we show the locations and relative sizes of the clumps from Williams et al. (1995).

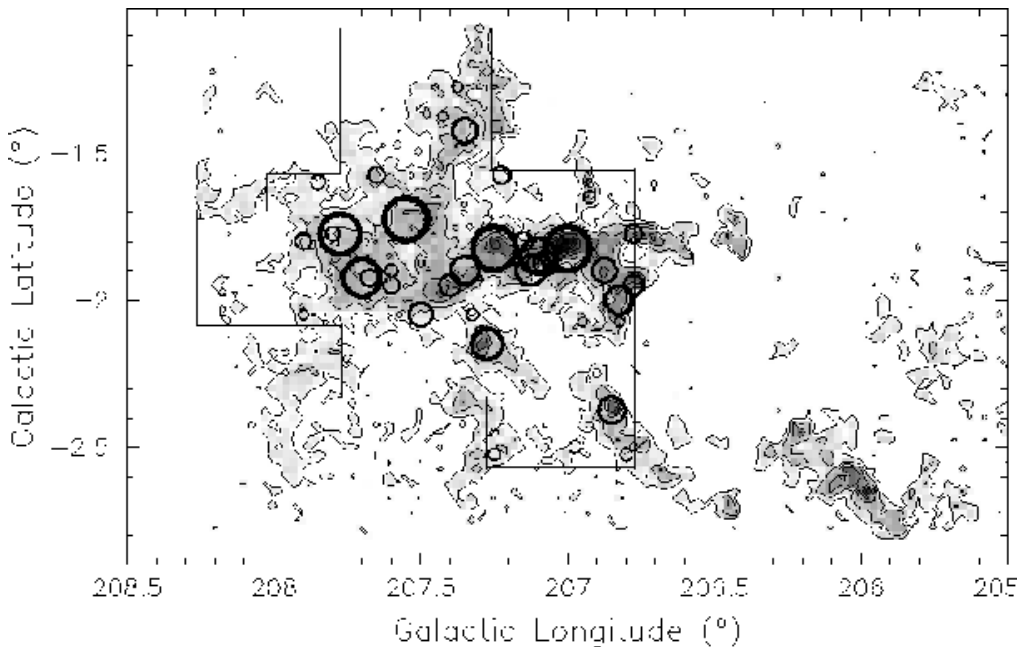


Figure 9. Locations and relative sizes of clumps in the Rosette Molecular Cloud from Williams et al. (1995). The size of the symbol is proportional to the mass of the clump. The contours represent CO emission from the survey of Blitz & Stark (1986), and the solid line delimits their coverage in  $^{13}\text{CO}$ .

From the clump central velocities Williams et al. (1995) found that the cloud has a well defined velocity gradient of about  $0.08 \text{ km}\cdot\text{s}^{-1}\cdot\text{pc}^{-1}$ . Also, the negative correlation between clump mass and clump to clump velocity dispersion suggested that the system is still far from equipartition even though it is dynamically evolved. Williams et al. (1995) also found the star forming activity to be more intense in the ridge and core areas, near the interface cloud-nebula: clumps located near the nebula presented larger excitation temperatures, average densities and star forming efficiencies, all clues of cloud evolution. Other properties of the clumps (mass, sizes and line widths) did not show any significant variations along the cloud.

Another CO study was done by Schneider et al. (1998a). The observations focused on the central part of the cloud, detailing the structure of the midplane star forming cores. They paid special attention to the IRS core, where the source AFGL-961 is located (see also Section 5.1) and pointed out the ample blue wing emission due to the powerful outflow from this object. In a complementary study, Schneider et al. (1998b) examined the CII emission ( $158 \mu\text{m}$ ) at the ridge, the central core and the IRS core. They found weak but significant  $\text{C}^+$  emission deep into the molecular cloud cores and suggested that the distribution agrees well with a clumpy molecular cloud exposed to a low level UV radiation field. The penetration of UV photons in the cloud is apparently facilitated by a high density contrast clump-interclump medium.

The clump mass spectrum in the Rosette Molecular Cloud has the form  $dN/dM \propto M^{-x}$  where  $x \approx 1.6$ , depending on the range, bin size and beam resolution used. The exponent in this power law is similar to other clouds (Blitz 1993), but what is more important, it is much shallower than the one corresponding to the stellar IMF ( $x = 2.35$ ). This shows that although there are more small clumps by number, most of the mass is contained in only a few big clumps, while for stars both numbers and total mass are dominated by the lowest mass bins. Interestingly enough, the power law index is in fact similar to that corresponding to the mass distribution function for embedded clusters, which is suggestive of a uniform star formation efficiency for most star forming cores (Lada & Lada 2003).

The more recent survey of Heyer, Williams, & Brunt (2006), obtained with the wide field array SEQUOIA at the FCRAO 14m telescope achieved resolutions of  $45''$  at 115 GHz and  $47''$  at 110 GHz. The maps revealed “textural variations” in the  $^{12}\text{CO}$  emission across the complex, with a brighter emission component within the nebula projected radius (approx. 30 pc from the center as defined by Celnik, 1985) and weaker, more extended emission outside this ionization edge. Heyer, Williams, & Brunt (2006) suggest that the weaker emission is probably due to subthermally excited material with lower densities. They also calculated the total molecular mass of the cloud to be  $1.6 \times 10^5 M_{\odot}$  from  $^{12}\text{CO}$ , and found a LTE mass of  $1.16 \times 10^5 M_{\odot}$  from  $^{13}\text{CO}$ . Moreover, they were able to apply a Principal Component Analysis (Heyer & Schloerb 1997) to determine the turbulent flows and the turbulence scale in the Rosette Molecular Cloud. The analysis revealed more significant variations in the velocity structure of the cloud at the regions located within the ionization than in the more diffuse, external component. This fact confirms the interaction of the cloud and the HII region. They suggested, however, that the interaction is still very localized, and have not affected the global dynamics of the cloud yet.

### 3.2. Interaction with the Rosette Nebula

Celnik (1986) focused on comparing his  $\text{H}\alpha$  map and radio continuum observations of the nebula (see Section 2.1) with the CO map of the molecular cloud from Blitz & Thaddeus (1980). Celnik constructed a complex model of the distribution of the main CO cores (see Fig 9) in the context of the HII region and estimated the rotation center of the cloud at  $(\alpha, \delta) = (6^{\text{h}}32^{\text{m}}39^{\text{s}}, +4^{\text{d}}19'43'', \text{J2000})$ . Finally, he re-calculated the mass of the entire complex by adding the total mass of ionized atoms, stars, dust and molecular gas, resulting in  $3.3 \times 10^5 M_{\odot}$ .

Another important study was done by Cox et al. (1990), who made use of the available infrared emission data from the IRAS satellite (12, 25, 60 and  $100 \mu\text{m}$ ). Cox et al. were able to study in great detail the distribution of dust and compared this to the dis-



tributions of ionized and molecular gas. Additionally, they were able to estimate a total infrared luminosity of roughly  $1.1 \times 10^6 L_{\odot}$ , or about 50% of the available luminosity from the cluster NGC 2244. Warm dust (usually present near an OB association) typically emits strongly at the four IRAS bands. However, Cox et al. showed that in the Rosette, while the 60 and 100  $\mu\text{m}$  emission are quite strong at regions of ionized and neutral gas (nebula), the 12  $\mu\text{m}$  emission is preferentially located beyond the limits of the ionization front (molecular cloud), suggesting a heavy rate of destruction of dust grains from UV radiation from the cluster. Surprisingly, the 25  $\mu\text{m}$  emission was found to be significant in some parts of the ionized nebula, possibly due to the existence of a second type of dust particle that is more resistant to UV photons. This was also suggested by Shipman & Clark (1994), who found that the maximum temperature in the shallow temperature gradient found in the nebula (see Section 2.1) seems too low to sublimate ice mantles in grains and too low for grains to emit significantly at 12 or 25  $\mu\text{m}$  — a problem possibly solved with a second type of grain in the region. Later, Shipman & Carey (1996) suggested that line emission could be contributing strongly to the IR emission of the nebula, and suggested once more that the presence of a “hot dust” component is necessary to model this emission, especially at 25  $\mu\text{m}$ .

Figure 10 shows the superposition of the 12  $\mu\text{m}$  emission from the IRAS survey and a 1400 MHz radio continuum emission map from Holdaway et al. (1999). The infrared contours indicate that the warm dust emission defines a shell that encloses the ionization front, showing the effect of heavy dust destruction by the nebula. The superposition of these maps defines very clearly the region where the HII bubble impacts the molecular cloud.

Patel et al. (1993) observed the SE quadrant of the nebula, which coincides with the regions located south and east of the Monoceros Ridge, where molecular globules were identified by Block (1990), Block et al. (1992) and Sugitani et al. (1991). The CO and  $^{13}\text{CO}$  ( $J = 1 \rightarrow 0$ ) data of Patel et al. confirmed that this part of the cloud contained nine well defined cometary globules, which appear to be blue-shifted by approximately  $6 \text{ km}\cdot\text{s}^{-1}$  with respect to the Rosette Molecular Cloud. The globules have sizes of 1-3 pc and masses of 50 to 300  $M_{\odot}$  and four of them are coincident with IRAS sources and local maxima in the  $^{13}\text{CO}$  emission. Patel et al. suggest that these globules cannot be formed as Rayleigh-Taylor instabilities as in the case of globules (elephant trunks) in the NW quadrant of the Rosette Nebula (see Section 5), but rather by a mechanism of radiation driven implosion, caused by penetration of UV radiation from the nebula cluster which favors D-type ionization fronts inside massive clumps, causing the formation of the globules. A follow up study by White et al. (1997) also included CO,  $^{13}\text{CO}$ , and  $\text{C}^{18}\text{O}$  observations of a similar region, revealing that the Globule 1 from Patel et al. is indeed the largest cometary globule in the area; this object has a prominent head-tail structure with a projected length of almost 1.3 pc which points away from the center of the Nebula. They also confirmed the agreement with a RDI model and were able to calculate an age of 0.4 Myr for the globule, suggesting that it has almost reached the stage of maximum compression and is close to a quasi-static cometary phase.

*High Energy Studies* When the Rosette Molecular Cloud was confirmed as a region of star formation, Gregorio-Hetem et al. (1998) used ROSAT data again, this time to map the MonR2 cluster and the Rosette Molecular Cloud areas in order to confirm a correlation between star forming cores and clusters of X-rays sources. They found strong X-ray emission in NGC 2244, at the ridge of the cloud (A1-2 in fig 8), and at the cloud core area (A1-1), but the resolution was poor and individual sources could not

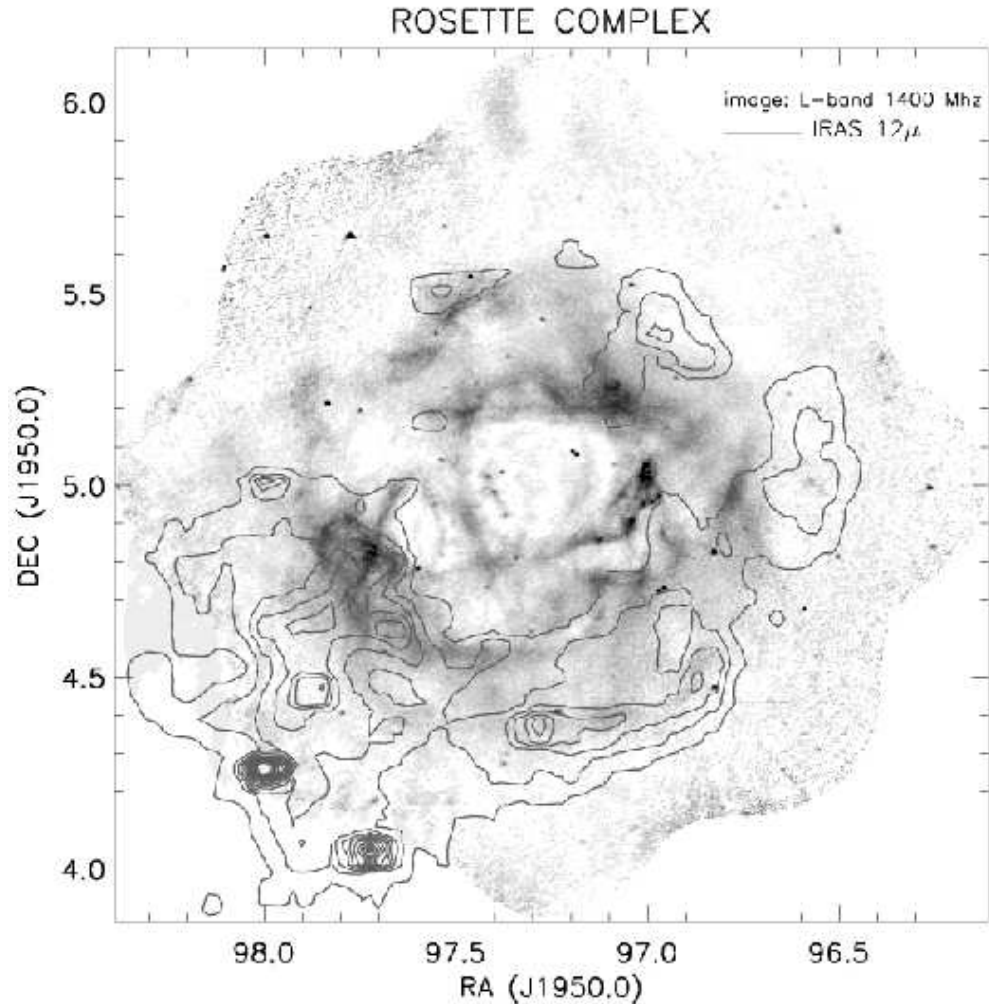


Figure 10. IRAS  $12\ \mu\text{m}$  emission map superimposed on a 1400 MHz radio continuum emission map. Credit: Holdaway et al. (1999) and NRAO.

be resolved. They suggested that molecular cores known to have active star formation but failing to show significant X-ray emission, could be predominantly forming low-mass stars. They also suggested that detectable X-ray counterparts are in most cases Herbig Ae/Be or T Tauri stars, as found in NGC 2244 (Li et al. 2002; Wang et al. 2008).

The more recent observations of the Rosette Complex done with Chandra (Townsend et al. 2003) have resolutions of only a few arcseconds, thus allowing for the detection of X-ray counterparts for 75% of the OB members of NGC 2244. One of the most interesting results of this study was the confirmation of a second, soft diffuse emission which probably originates from the O star winds and is later brought to thermalization by wind-wind interactions or by the shock with the surroundings, in this case the molecular cloud (see Figure 11). This X-ray plasma surrounds the OB association and fills the nebula cavity completely.

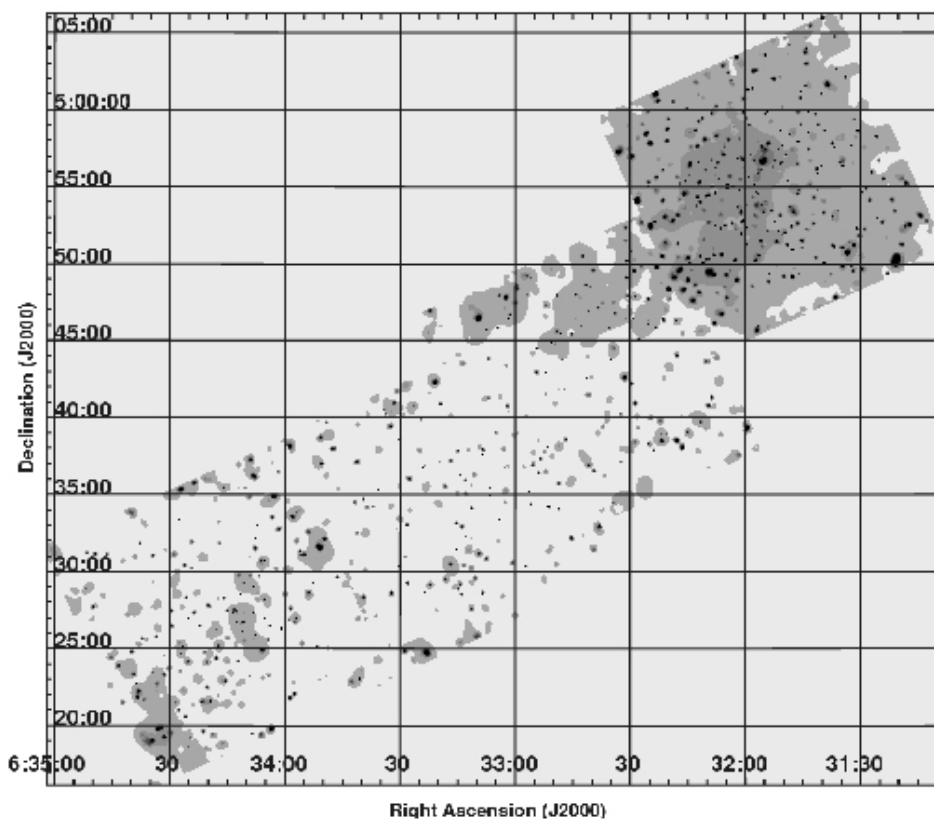


Figure 11. A 0.5-2 keV Chandra image of the Rosette Complex. The emission has been smoothed to highlight the soft diffuse emission that originates in the nebula and propagates into the molecular cloud. Credit: Townsley et al. (2003) and NASA/Chandra X-Ray Observatory.

The Rosette Nebula may not only be interacting with its companion molecular cloud. The location of the Rosette Nebula near the edge of the Monoceros Loop (Davies 1963) — also known as the Monoceros Supernova Remnant — at the edge of the NE quadrant, has motivated a number of studies aimed at investigating the high energy photon emission in that region. Deep  $H\alpha$ + $[NII]$  photographic plates by Davies et al. (1978) suggested a correlation between a filamentary structure observable in  $H\alpha$  emission and a Rosette nebula feature observable in 240 MHz radio waves. This feature was proposed as evidence of loop-nebular interaction and confirmed by decameter (Odegard 1986) and diffuse X-ray emission (Leahy et al. 1986) observations. Later, high energy (100 MeV)  $\gamma$ -ray images from EGRET (Jaffe et al. 1997), revealed a feature partly coincident with the filaments and apparently significant ( $7\sigma$ ) over expected diffuse emission. If real, this  $\gamma$ -ray feature would possibly be due to the interaction of charged particles with the dense ambient medium at the shock region. The HEGRA system of atmospheric Cerenkov telescopes at La Palma Observatory was used to calculate the cosmic ray emission from the loop-nebula interaction region, and found one possible TeV emission source (3EG J0634+0521) with low statistical significance (Aharonian et al.

2004). More recently, the HESS telescope array in Namibia was used again to map the SNR-Nebula interaction region and found one gamma ray source, HESS J0632+057, located close to the rim of the Monoceros Loop (Aharonian et al. 2007).

### 3.3. The Rosette Molecular Cloud: Embedded Populations

*Near-infrared Observations* The coincidence of massive clumps and luminous IRAS sources pointed out by the study of Williams et al. (1995) strongly suggested that star formation had already taken place across the molecular cloud. However, the poor spatial resolution of the IRAS point source survey did not allow the resolution of individual members of an embedded population. Early near-infrared studies (e.g. Pérez et al. 1987) did not cover the molecular cloud areas, and optical photometric studies were incapable of detecting obscured populations.

An exploratory near-infrared survey (JHK) by Phelps & Lada (1997) that made use of the imager SQUID finally confirmed the existence of embedded clusters in some of the most massive clumps from the list of Williams et al. that were associated with an IRAS source. Phelps & Lada were able to identify by visual inspection of their images seven deeply embedded clusters with bright nebulosities. Other massive clumps did not contain a cluster, which suggests that high mass is a necessary but not a sufficient condition for cluster formation.

Complete spatial coverage of the Rosette Complex in the near-infrared was first accomplished with the release of the All-Sky 2MASS survey catalogs. The 2MASS survey was a major gain in data uniformity but unfortunately not in sensitivity. Due to the distance to the Rosette ( $1.6 \pm 0.2$  kpc), the 2MASS completeness limit ( $K=14.3$  mag) is not deep enough to study the low mass end of the IMF. Li & Smith (2005) studied the distribution of 2MASS sources with large H-K colors and they were able to suggest three general areas of cluster formation. The extensions of these star formation regions were defined visually, and could not be compared with the clusters of Phelps & Lada (1997) because at that point the extents and membership of individual clusters were not determined.

The survey of Román-Zúñiga et al. (2008) aimed for deeper observations using FLAMINGOS on the KPNO-2.1m. The project was done as part of a FLAMINGOS/NOAO survey of Giant Molecular Clouds <sup>2</sup>. Observations of the Rosette covered the regions surveyed by Phelps & Lada and extended to the Back Core and the nebula. Identification of young embedded populations was done by selecting objects with near-infrared excess characteristic of circumstellar emission. Also, a Nearest Neighbors analysis was applied to this color selected sample to facilitate the detection of embedded clusters as regions with significant local surface densities.

The technique allowed for a clear confirmation of the location and extensions of the seven bright clusters reported in Phelps & Lada, labeled as PL01 to PL07, but also indicated the existence of another two clusters associated with massive clumps in the molecular cloud, labeled as REFL08 and REFL09. The sources with near-infrared excess also traced well the extension of NGC 2244 and a possible new cluster at the western edge of the HII bubble, located at the region historically identified as NGC 2237, (see also Section 2.2). Finally, a small cluster was detected at the northeast end of the

---

<sup>2</sup>see <http://flamingos.astro.ufl.edu/sfsurvey/sfsurvey.html>

nebula and was labeled REFL10. The location of the clusters and their distribution of near-infrared excess sources is shown in Figure 12.

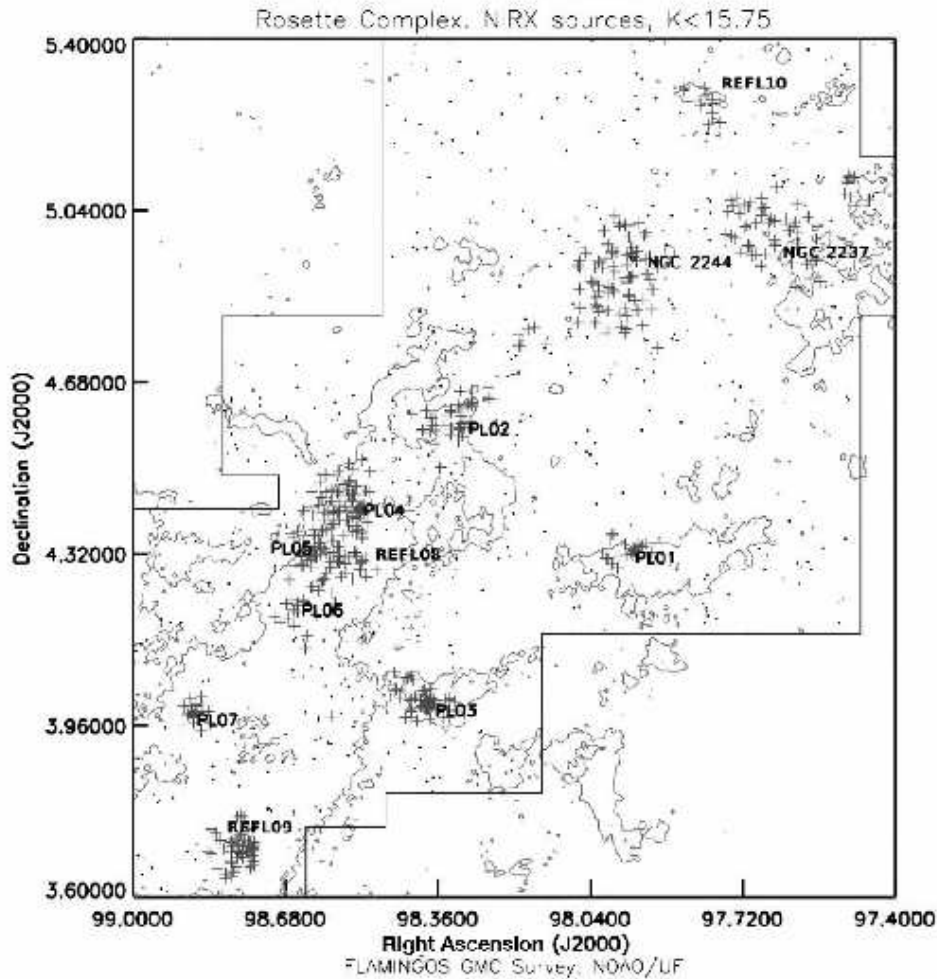


Figure 12. Identification of young clusters in the Rosette Complex. Plus symbols indicate the location of NIRX objects brighter than  $K < 15.75$  and local surface densities higher than the background average. Black dots are sources with near-infrared excess colors and local surface densities below the background average. The contour levels indicate a baseline level ( $0.8 \text{ K} \cdot \text{km} \cdot \text{s}^{-1}$ ) of  $^{13}\text{CO}$  emission from the survey of Heyer, Williams, & Brunt (2006) used to define the projected surface of the cloud. The thin solid line marks the coverage of the FLAMINGOS survey.

The sizes (equivalent radii) of clusters in the Rosette are relatively large, appear to be anti-correlated with their mean average extinctions, and with the near-infrared excess fractions. If larger near-infrared excess fractions indicate slightly younger ages, then the anti-correlation might be indicative of rapid cluster evolution: clusters could form as compact units then expanded in a timescale shorter than the T Tauri phase.

From the direct counting of near-infrared excess stars, it was possible to determine the fraction of the young stellar population that is forming in clusters at the present day. The 9 largest clusters embedded in the Rosette Molecular Cloud occupy approximately  $242 (')^2$  or approximately 9% of the main molecular cloud areas covered by the FLAMINGOS survey. After correcting for background stars the embedded clusters account for  $86\pm 5\%$  of the embedded population in the cloud. These fractions are comparable to what was found in other nearby molecular clouds like Orion or Perseus (Lada et al. 1991; Carpenter 2000), where clusters comprise 50 to 96% of the young stars that can be observed.

Table 3. Young Clusters in the Rosette Complex

ID <sup>a</sup>	RA <sup>b</sup>	DEC <sup>b</sup>	Clump <sup>c</sup>	$R_{clump}$ <sup>d</sup> [pc]	No. IRX <sup>e</sup> K<15.75	No. Class I <sup>f</sup> M<0.4 M <sub>⊙</sub>	$R_{eq}$ <sup>g</sup> [pc]
	(J2000)						
PL01	06 31 49.32	+04 19 34.7	11	2.21	29±5	9	1.16
PL02	06 33 16.78	+04 35 32.1	18	1.33	32±6	12	1.46
PL03	06 33 33.07	+04 00 11.2	7	2.79	80±9	>6	1.69
PL04	06 34 13.92	+04 25 05.4	1	2.36	89±9	<107 <sup>h</sup>	1.85
PL05	06 34 30.70	+04 20 01.8	19	1.50	57±8	<107	1.31
PL06	06 34 38.76	+04 12 55.4	2	3.06	13±4	>10	0.75
PL07	06 35 29.78	+03 59 10.9	3	2.79	22±5	27	0.88
REFL08	06 34 18.98	+04 20 03.6	17	1.71	49±7	<107	1.30
REFL09	06 35 07.73	+03 41 34.7	5	3.60	65±8	12	1.49
PouC	06:33:12.68	+04:31:00.5	—	—	—	12	0.90
PouD	06:33:40.98	+04:03:56.1	—	—	—	9	0.83
REFL10	06 31 06.79	+05 14 50.0	—	—	15±4	—	1.15
NGC 2237	06 31 58.51	+04 54 35.7	—	—	36±6	—	1.91
NGC 2244	06 30 36.10	+04 58 50.6	—	—	62±8	176	2.30

<sup>a</sup> ID key: PL—Phelps & Lada (1997); REFL—Román-Zúñiga et al. (2006a); Pou—Poulton et al. (2008)

<sup>b</sup> Location of peak surface density of near-infrared excess sources

<sup>c</sup> Molecular clump host identification from Williams, Blitz & Stark (1995)

<sup>d</sup> Clump host equivalent radius

<sup>e</sup> Limited to K<15.75 mag.

<sup>f</sup> Adapted from Table 2 and figure 9 of Poulton et al. (2008). Mass detection limit is 0.4 M<sub>⊙</sub>

<sup>g</sup> Cluster radii defined from IRX local surface density contours, except PouC and PouD, listed as equivalent radius.

<sup>h</sup> Clusters PL04, PL05 and REFL08 are reported as a single cluster in Poulton et al.

*Mid-infrared Observations* Recently, Poulton et al. (2008) reported the first results of the Spitzer telescope survey of the Rosette Molecular Cloud. The area surveyed with IRAC and MIPS covers  $1\times 1.5^\circ$ , similar to the one studied with FLAMINGOS. The Spitzer observations allowed to identify, via the fit of SED profiles, a total of 751 young stellar objects with infrared excess down to a mass limit of 0.4 M<sub>⊙</sub>. Also, they used a method of nearest neighbors applied to all sources with infrared excess to identify embedded clusters, confirming the seven clusters of Phelps & Lada (1997) as the major clusters in the cloud and confirming the existence of clusters REFL08 and REFL09 (labeled as clusters E and F, respectively). Their analysis also revealed two new small

clusters or associations, labeled clusters C and D (we used the labels PouC and PouD in this work). These two groups are located near clusters PL02 and PL03, respectively.

The Spitzer survey of the Rosette confirmed that Clusters PL01 to PL05 have very dense envelopes of hot dust, evidenced by strong extended emission in all IRAC and MIPS bands. The Spitzer survey also revealed that sources within 15 pc from the center of NGC 2244 are definitely older than those deeply embedded in the cloud, with 2% vs 7% of identified Class I sources, respectively.

In Figures 13, 14, 15 and 16 we present false color images constructed with near-infrared images from FLAMINGOS and with mid-infrared images from IRAC for all the embedded clusters in the Rosette Molecular Cloud: PL01-07, REFL08-09 and PouC-D. The FLAMINGOS images, with higher resolution, define well the stellar content of the clusters, while the IRAC images show in addition the distribution of hot dust and gas around the embedded clusters.

Table 3 contains information about the location of the 14 known clusters embedded in the Rosette Molecular Cloud, along with the corresponding clump from Williams et al. (1995). Also indicated is the number of near-infrared excess stars detected in each cluster region and the cluster equivalent radii, which was calculated by estimating the extension of each cluster from local surface density contours of near-infrared excess sources above the background level. We also indicate the number of Class I sources reported by Poulton et al.

*Interaction of Embedded Populations with the Local Environment* In order to give insight into the nature of the embedded populations of the Rosette Molecular Cloud, a high resolution mm-wave survey of clusters PL01 to REFL08 was performed at the IRAM 30m telescope (Román-Zúñiga 2006, Román-Zúñiga, Williams & Lada, 2008 (in prep)). The cluster regions were scanned for emission in 6 molecules:  $^{12}\text{CO}(2-1)$ ,  $^{13}\text{CO}(2-1)$ ,  $\text{C}^{18}\text{O}(2-1)$ ,  $\text{CS}(2-1)$ ,  $\text{HCO}^+(1-0)$  and  $\text{N}_2\text{H}^+(1-0)$ . All of the clusters show prominent clumps in most tracers, except cluster PL02 which has weak emission in  $\text{C}^{18}\text{O}(2-1)$  and  $\text{N}_2\text{H}^+(1-0)$ . In Figure 17 we show one example of the maps of dense gas emission maps for cluster PL06 (host of AFGL 961).

Bulk physical properties of the clumps are calculated from these observations. Particularly, mass, sizes and velocity dispersions appear to be fairly similar for all of the cluster areas, which translates to no significant variation of the properties of star forming clumps across the cloud, as suggested by Williams et al. (1995). However, the morphology of the gas emission is different from clump to clump, suggesting different stages of the clusters evolution. For example, while the gas emission around clusters PL01, PL06, PL07 and REFL08 is compact and forms a well defined envelope around the clusters, clusters PL03, PL04 and PL05 appear to be partially emerging from the clumps, with the gas apparently being swept out from some areas of the cluster and recollected in others.

The emergence of the massive clusters PL04 and PL05 might suggest a late stage of embedded cluster evolution. The emission of dense gas tracers for these clusters is confined to only two relatively small areas which coincide with the most obscured and dense parts of the respective cores. The rest of the stars in the clusters are still embedded in the larger and more quiescent  $^{13}\text{CO}$  core but some of them are already visible in DSS optical plates. Clusters PL04 and PL05 are the largest and most extended embedded clusters in the Rosette Molecular Cloud (see Table 3) but could also be the oldest. These clusters are located in the part of the cloud that is in direct interaction with the shock front from the Nebula, as described by Heyer, Williams, & Brunt (2006).

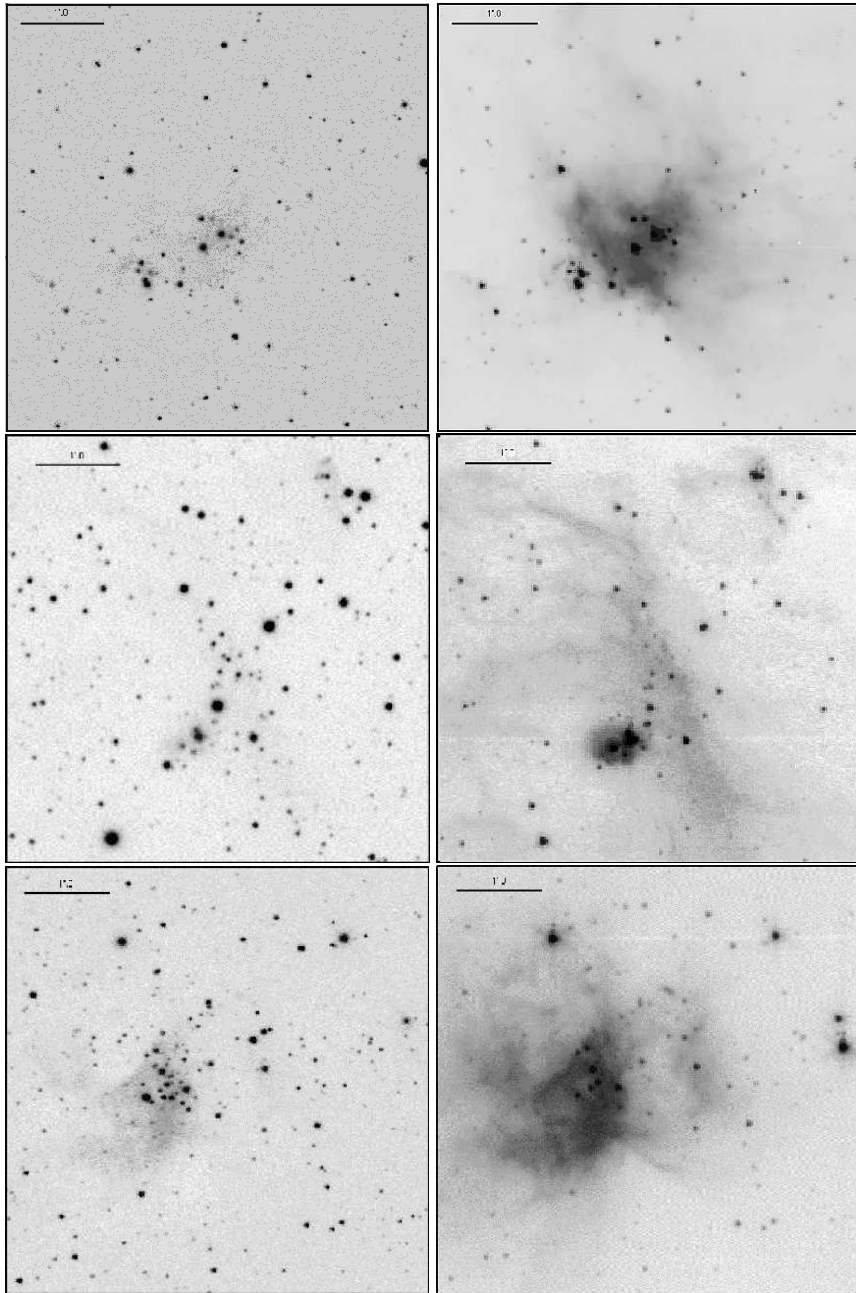


Figure 13. Embedded clusters PL01, PL02 and PL03 (top, middle and bottom, respectively) in the Rosette Molecular Cloud. *Left Panels:* False 3 color images (J,H,K) constructed with images from the FLAMINGOS survey. *Right Panels:* False 3 color images ([3.6],[4.5] and [8.0] $\mu\text{m}$ ) constructed with images from the IRAC survey. All images cover a  $5' \times 5'$  area. Scale bars of 1.0 arcmin are also shown on top.



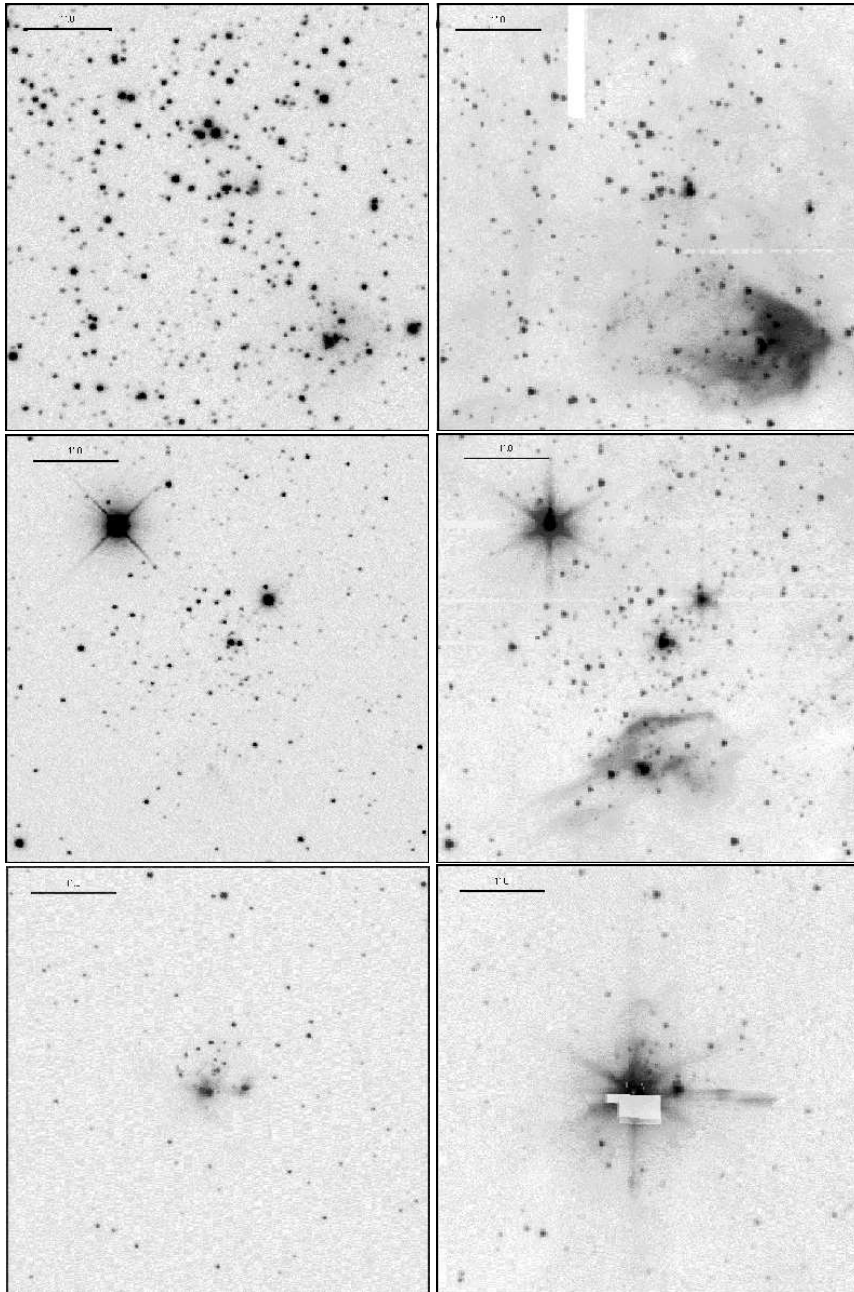


Figure 14. Same as figure 13, for embedded clusters PL04, PL05 and PL06 (top, middle and bottom, respectively). Note: Artifacts in cluster PL06 IRAC image are due to saturation of IRAC detector by the bright source AFGL961.

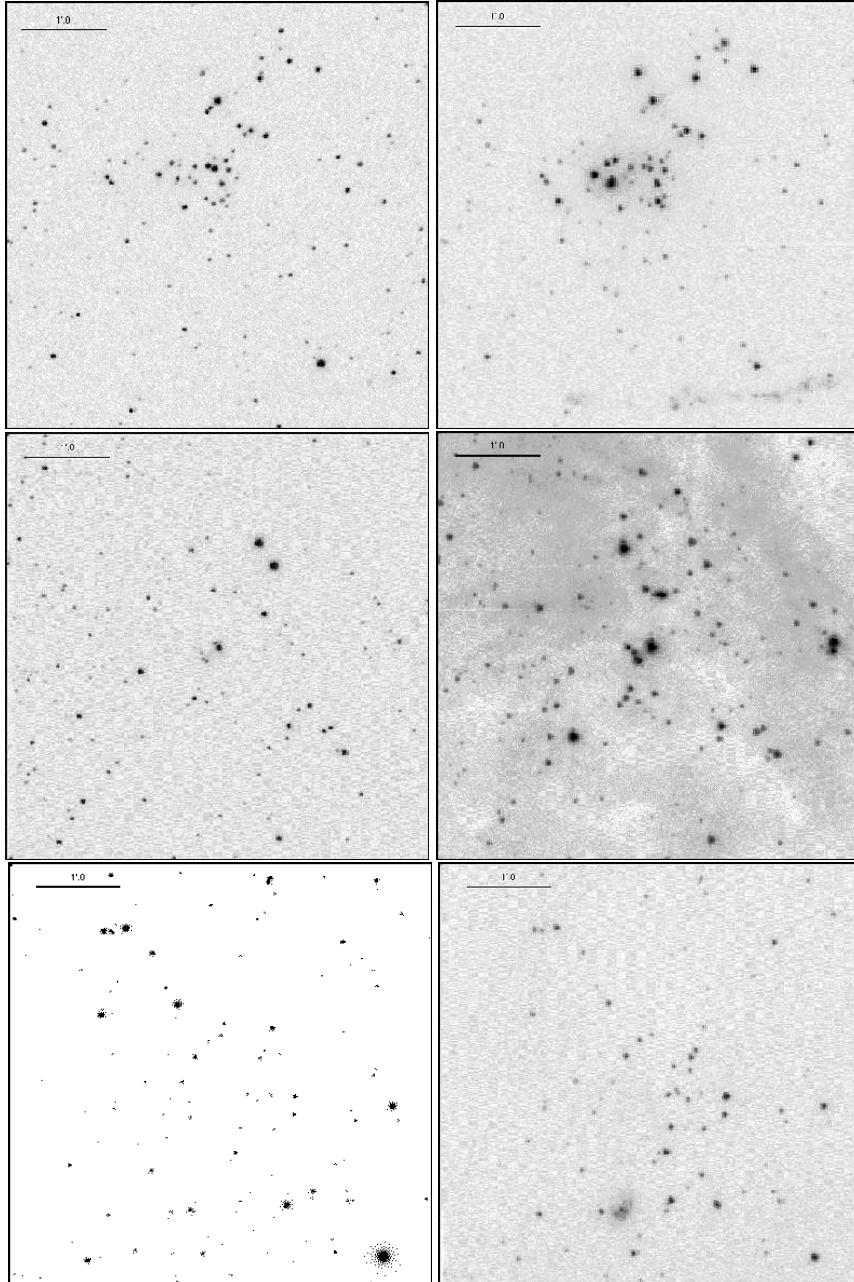


Figure 15. Same as figure 13, for embedded clusters PL07, REFL08, and REFL09 (top, middle and bottom, respectively). Note: IRAC picture for REFL09 was constructed with [4.5], [5.0] and [8.0]  $\mu\text{m}$ , as it misses coverage in [3.6]  $\mu\text{m}$ .

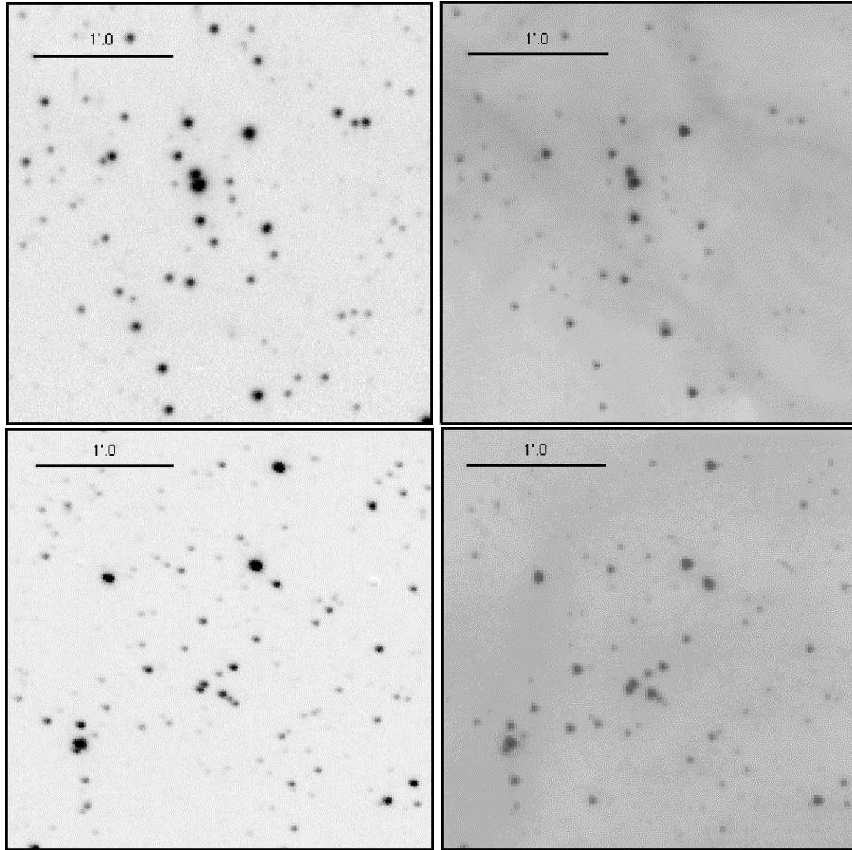


Figure 16. Same as figure 13, for embedded clusters PouC and PouD (top, and bottom, respectively). Note: The area covered in these images is  $3' \times 3'$ .

*The Sequential Formation Hypothesis* In Figure 18 we show the distribution of the surface density of near-infrared excess sources (young stars) in the Rosette Complex as a function of the distance from the center of NGC 2244, as calculated by Román-Zúñiga et al. (2008). Young clusters appear as peaks in this distribution, and it is possible to distinguish four main groups of clusters. The most prominent group contains NGC 2244, NGC 2237 and REFL10, which are the clusters located in the nebula. The second group contains clusters PL01 and PL02 and coincides with the cloud ridge (core A1-2). The third group contains clusters PL04, PL05, REFL08 and PL06, all located at the RMC central core, and cluster PL03 located in core D. The fourth and last group contains clusters PL07 and REFL09 which are located at the back core of the cloud. In the bottom panel of Figure 18 we show the average infrared excess fraction for each of these cluster groups. The average excess fraction appears to increase as a function of distance from NGC 2244, suggesting that the embedded clusters are progressively younger the further they are from the Nebula.

The existence of this apparent age sequence indicates that star formation in the Rosette did indeed take place sequentially in time, but not in the way proposed by Elmegreen & Lada (1977), because that model requires one episode of cluster formation to trigger the next one. The relative age differences of clusters cannot be large

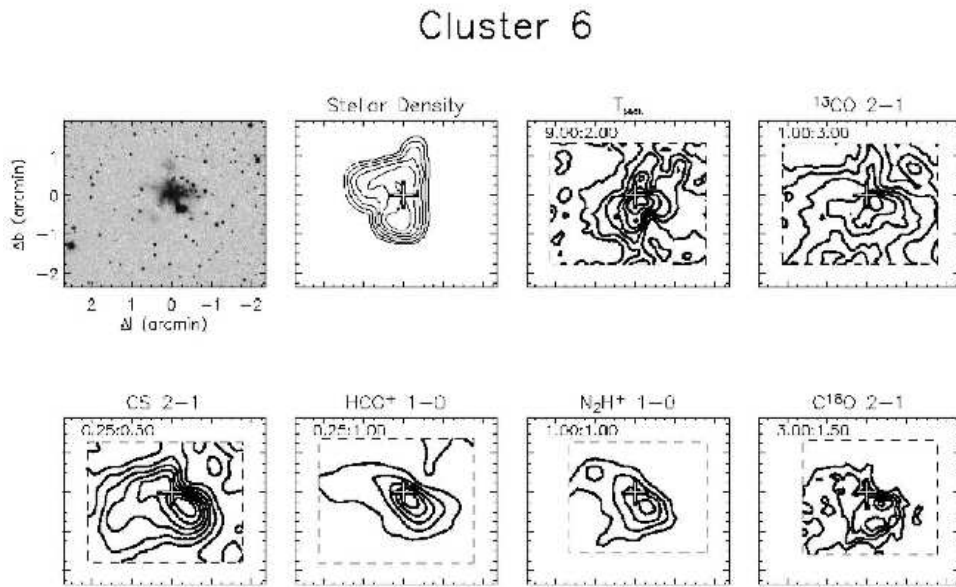


Figure 17. Maps of dense molecular gas emission towards cluster PL06 in the Rosette Molecular Cloud, from Román-Zúñiga (2006). The first two panels show a false color near-infrared image of the cluster and a IRX surface density map. The molecular map panels have base and step values for the contour levels. The maps are integrated intensity except for  $^{12}\text{CO}(2-1)$  which is mapped as peak temperature.

enough to account for such a scenario. Instead, it appears that the overall age sequence of cluster formation may be primordial, possibly resulting from the formation and evolution of the molecular cloud itself. The HII region cannot be responsible for the sequence of cluster ages, although it does appear to have a significant impact on the underlying sequence by either enhancing or inhibiting the star forming process: At the cloud ridge, the direct interaction with hot, ionized gas might contribute to the rapid evaporation of cluster envelopes in PL01 and PL02, possibly stopping the star formation process at an early stage; however, recent Chandra and Spitzer telescope observations (Wang et al. (in prep); Poulton et al., 2008) suggest that PL02 hosts two Class 0/I sources, which is suggestive of cluster substructures younger than PL04 or PL05. At the central core, where the main interaction between the nebula and the molecular cloud takes place, the result is an enhancement of the star formation efficiency, evidenced by the fact that the clusters in this area (PL04, PL05, PL06, REFL08) account for almost 50% of the total embedded population in the cloud. Finally, at the back core the influence of the HII region is minimal and star formation in this part of the cloud may have occurred spontaneously (Román-Zúñiga et al. 2008; Poulton et al. 2008).

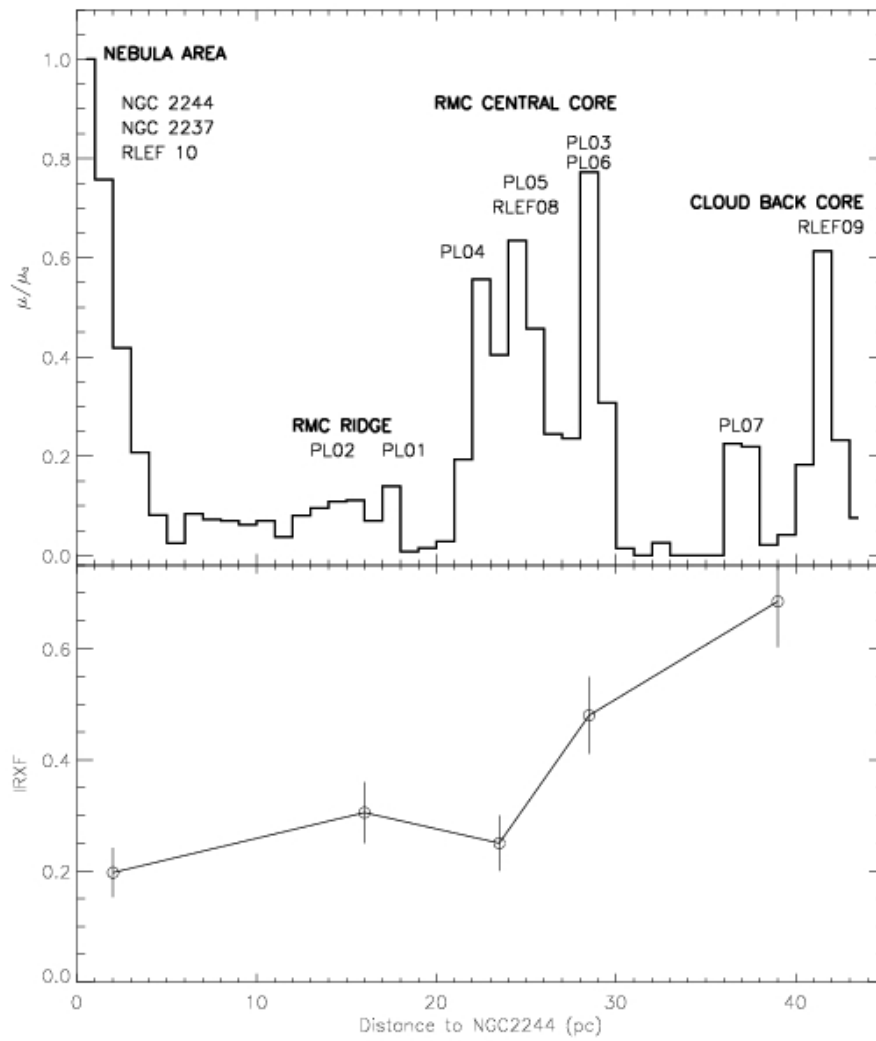


Figure 18. Top panel: Distribution of near-infrared excess source density as a function of distance from the center of the Rosette Nebula (NGC 2244). The counts are made in sectors of 1.0 pc in length and counts in each sector have been scaled and normalized to the area and counts in the central 1.0 pc circle in NGC 2244. Labels indicate the approximate locations of embedded clusters as well as the main 'regions' of the complex, defined by Blitz & Thaddeus (1986). Bottom panel: averaged near-infrared excess fractions in each of the cluster groups defined from the top plot appear to increase with distance from the Rosette Nebula. From Román-Zúñiga et al. (2008).

## 4. Regions of Particular Interest

### 4.1. AFGL 961. Cluster PL06

Particular attention in the literature has been given to cluster PL06, associated with the bright infrared source AFGL961. The source was originally identified by Cohen (1973), who also obtained its spectral energy distribution from 2 to 18  $\mu\text{m}$ . This distribution was later extended to include measurements at 53, 100 and 175  $\mu\text{m}$  by Harvey et al. (1977). Blitz & Thaddeus (1980) found that the CO emission towards the source is strongly self absorbed and presents broad wings, evidence of a violent interaction of the central source with the molecular envelope. These characteristics were confirmed by Lada & Gautier (1982); Loren (1981); Schneider et al. (1998a); Heyer, Williams, & Brunt (2006) and Román-Zúñiga (2006). The powerful CO outflow that generates the wings was measured to have a gas kinetic energy close to  $10^{47}$  ergs, and is moving almost 19  $M_{\odot}$  of material (Lada & Gautier 1982). The outflow is bipolar and spectral signatures revealed that the outflow is in fact caused by an ionized wind. The self absorption is possibly caused by a foreground layer of colder material, and in fact, infrared spectra at 1  $\mu\text{m}$  and 1 mm obtained by Cox (1989) revealed the presence of ice bands towards the source, confirming the effect.

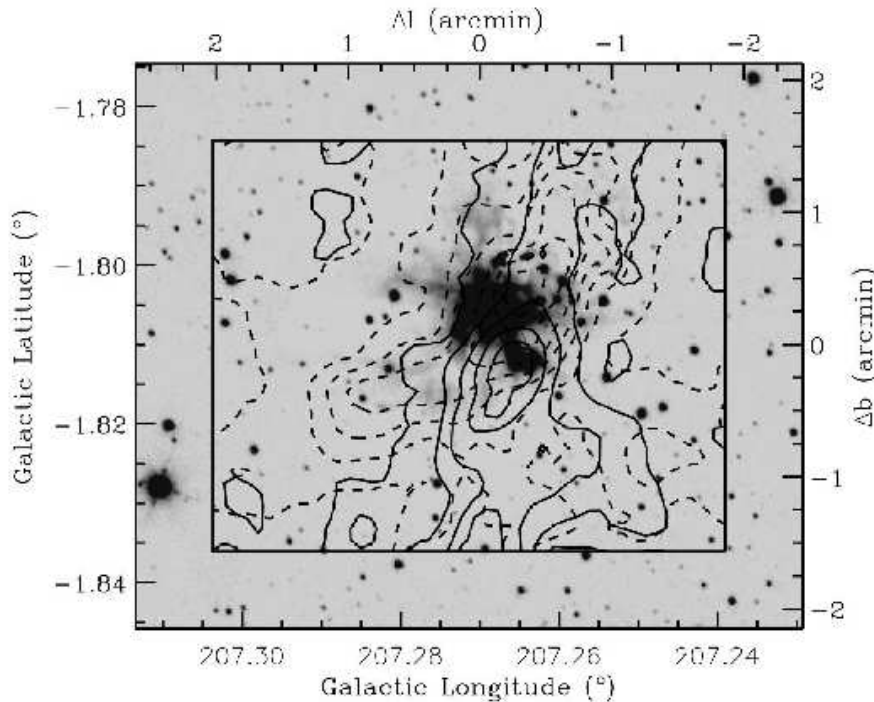


Figure 19. A FLAMINGOS near infrared image overlaid with contours of  $^{12}\text{CO}(2-1)$  outflow (line wings) emission towards cluster PL06 which hosts the massive PMS binary AFGL961. The solid contours show integrated emission from 5 to 8  $\text{km}\cdot\text{s}^{-1}$ , and the dotted contours show integrated emission from 17 to 20  $\text{km}\cdot\text{s}^{-1}$ .

The central source in AFGL961 is a B type PMS binary with a separation of approximately 0.05 pc, hence the common nomenclature AFGL961a and AFGL961b,

which refer to the eastern and western component, respectively. Near infrared observations (Aspin 1998; Román-Zúñiga et al. 2008) revealed that approximately another 30 young sources are associated with this cluster, and Aspin (1998) was able to demonstrate that at least 9 of these sources were associated with shock-like features which corroborated the strong interaction with the local medium.

Figure 19 combines a FLAMINGOS image with  $^{12}\text{CO}(2-1)$  data from the Román-Zúñiga (2006) survey in the form of integrated intensity contours. Self absorption is evident even in the averaged spectra, and the red and blue wings appear to confirm the existence of two different components of the gas outflow, although none of them are highly collimated.

#### 4.2. Jets, Knots, Elephant Trunks and Globules

The [SII] survey of Ybarra & Phelps (2004) revealed 13 regions of excited gas, 3 associated with external excitation from winds of NGC 2244 sources and 10 associated with winds from young sources in the embedded clusters of the molecular cloud. Most of the main clusters host one of these [SII] features, all reminiscent of HH objects and thus suggestive of strong interaction of young sources with their surrounding medium or at least of a high frequency of collimated outflows from young sources. Counterpart near infrared  $\text{H}_2$  observations (Phelps & Ybarra 2005) revealed that one source in the [SII] study, RMC-C (06315690+0419026) could be in fact a Class I object associated with a large outflow designated HH 871. The source is very close to cluster PL01 and could be associated with it. See Figure 20.

A series of studies by Meaburn & Walsh (1986), Clayton & Meaburn (1995) and Clayton et al. (1998) were dedicated to the investigation of a group of dense dense nebulous knots located at the south eastern edge of the HII cavity in the nebula area at approx.  $(\alpha, \delta) = (6^{\text{h}}29^{\text{m}}36^{\text{s}}, +5^{\text{d}}00'00'')$ , J1950). In the first paper, Meaburn & Walsh obtained  $\text{H}\alpha$ + [NII] filter photographs of the central cavity areas and combined them with echelle spectroscopy data. They suggested two possibilities for the origin of the knots: a) they are HH objects propelled by T Tauri sources with bipolar activity, or b) they are bow shocks around dense globules overtaken by large wind driven shells.

In the second study, Clayton & Meaburn generated a data cube of [OIII]5007 Å profiles obtained by scanning the knot areas with a multi-slit echelle spectrometer. They noticed that the largest knot, labeled C, is indeed very bright in this line, and suggested again that the feature might originate from a low mass young star. In their third study, Clayton et al. studied again the prominent knot C. The combined observations plus K band images identified candidates for the driving sources, and proposed that the top group of knots — which appear to coincide with K band sources — are all associated with a giant Herbig-Haro flow. The large scale of the corresponding outflow would be consistent with the idea of a large jet associated with the source RMC-C (see Figure 20), thus confirming the existence of parsec scale flows in the Rosette. Several FLAMINGOS sources lie in the area and the knots are barely visible in J and H, so a very interesting follow up would be to determine if any other faint sources are also associated with the knots. Also, Meaburn et al. (2005) found a possible microjet associated with a low mass young star, and most likely observable due to the Ly- $\alpha$  emission of the nebula.

Li (2003) and Li & Rector (2004) reported the discovery of two cometary jet systems with external irradiation. These two objects were recently catalogued as HH 889 and HH 890 (see <http://casa.colorado.edu/hhcat/>). These jets are immersed in the pho-

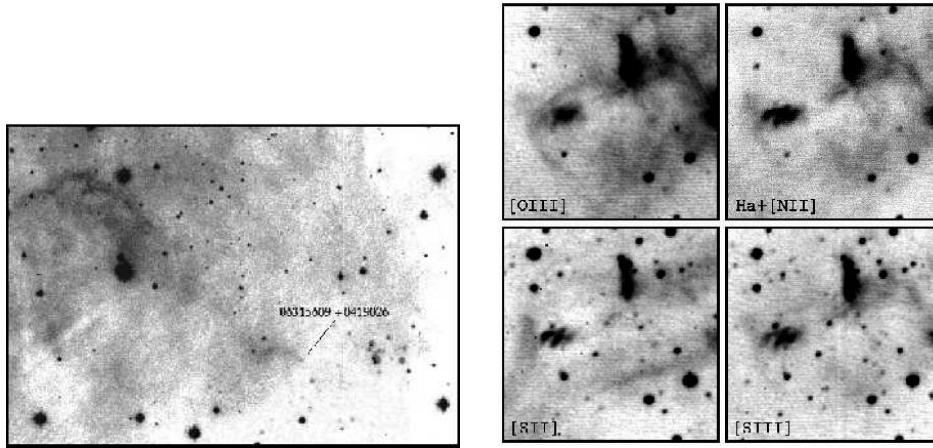


Figure 20. Large outflows and knots in the Rosette Complex environment. The left side panel is a composite [SII]-2MASS image of object HH 871 and its associated source Rosette Molecular Cloud-C from Phelps & Ybarra (2005). The right panel shows a group of conspicuous knots in the inner western edge of the HII region. From Clayton et al. (1998).

toionized region and thus are awash by heady UV radiation, which apparently results in an interesting set of bow shock structures. Given the age of NGC 2244, there is an upper limit of 1-2 Myr in the timescale of the jet production. Interestingly, the objects associated as the driving sources present no infrared excess Li (2005), which suggests a very rapid disk dissipation, with timescales of  $10^3$  to  $10^4$  yr (Li et al. 2007), leading to a rapid transition from CTTS to WTTS stages (Li & Rector 2007). These aspects pose interesting questions about the environmental dependence of the mechanisms of jet formation and also suggest that CTTS and WTTS objects can be spatially mixed in regions of massive star formation.

At the northwestern edge of the central cavity in the Rosette Nebula, there is a large group of prominent dusty pillar structures or *elephant trunks* (Herbig (1974), see Figure 21). Schneps et al. (1980) observed this region in CO and  $^{13}\text{CO}$  ( $J=1\rightarrow 0$ ), and found that the morphology of the molecular gas emission in the area follows very closely the optical outline of the pillar features. A very interesting fact is that the physical properties of the globules associated with the larger pillar structures are not different from those of globules in clouds not associated with HII regions. Individual globules in the area have  $\text{H}_2$  densities of  $\sim 10^4 \text{ cm}^{-3}$  and temperatures of  $\sim 10$  K. The trunks have velocity gradients of up to  $1.1 \text{ km}\cdot\text{cm}^{-1}(\prime)^{-1}$ , oriented along their direction of elongation and these gradients might be responsible for the morphology. The “stretching” of the trunks might have a time scale of  $\sim 3$  to  $6 \times 10^5$  yr, which is consistent with the dynamical age of the HII region given an expansion rate of  $20 \text{ km}\cdot\text{s}^{-1}$ .

Later, the studies of Carlqvist et al. (1998; 2002) were dedicated to study the internal structure of the elephant trunks. By constructing an extinction map of the largest trunk from a B-band CCD image, they were able to identify a clear helical structure, which they suggest might originate from an alignment with a primordial helical magnetic field (magnetic rope model). If true, this magnetic field would be present before the HII region was formed, and it could be responsible for maintaining the trunk-system



and would explain the observed velocity gradient even after erosion from the winds of NGC 2244.

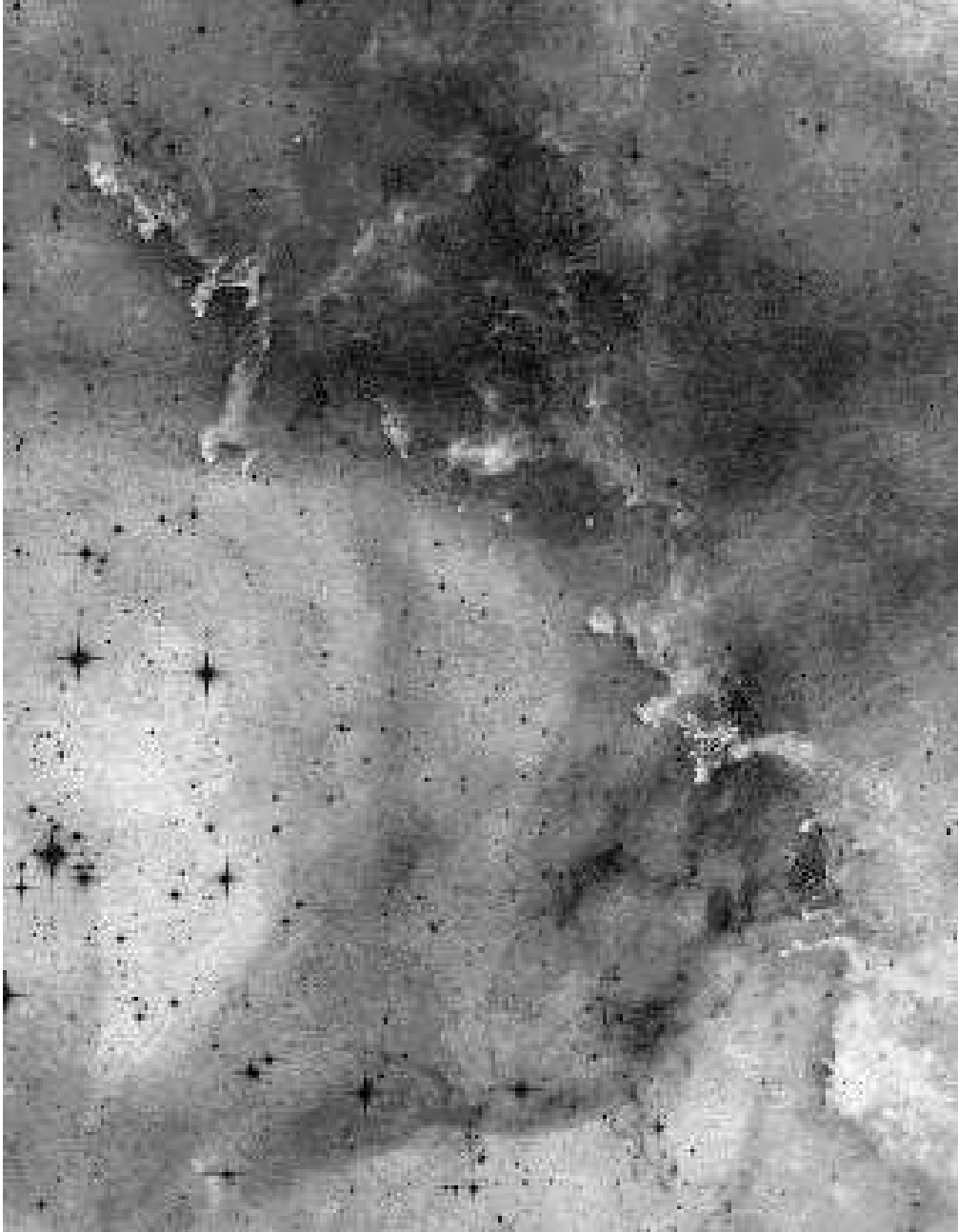


Figure 21. The northwestern edge of the cavity in the Rosette Nebula showing a complex system of pillars, trunks and small globules. Credit: Ignacio de la Cueva Torregrosa.

Gonzalez-Alfonso & Cernicharo (1994) observed 4 of the densest ‘teardrops’ located at the tips of the elephant trunks. Using the IRAM 30m telescope they found significant emission in  $^{12}\text{CO}(1-0$  and  $2-1)$ ,  $^{13}\text{CO}(1-0$  and  $2-1)$  and  $\text{CS}(2-1$  and  $3-2)$ . They confirmed kinetic temperatures for the globules between 15 and 20 K and masses between  $0.02$  and  $0.5 M_{\odot}$ . The  $^{12}\text{CO}$  line profiles had significant outflow (wing) components, possibly indicating the pressure exerted by the ionized gas in the HII region on the neutral gas of the teardrops. Recently, Gahm et al. (2007) made a complete survey of the entire chain of dark trunks in the northwest edge of the central cavity. They observed 23 fields in  $\text{H}\alpha$  using the 2.6m Nordic Optical Telescope, obtaining images of filaments and globules at a resolution of  $0.188 \text{ pix}^{-1}$  (about 300 AU at  $d = 1600 \text{ pc}$ ). The observations revealed a total of 145 individual small globules, many of them located in isolation near large pillars. They were able to obtain density profiles for the globulettes by converting from  $A_{\alpha}$  extinction, and showed that most objects agreed well with  $r^{-1.5}$  configurations typical of protostellar conditions. The total densities of the globules varied from  $3 \times 10^3$  to  $1 \times 10^5 \text{ cm}^{-3}$  and values of total mass assuming uniform density were found to agree well with those obtained for the few counterparts from the survey of Gonzalez-Alfonso & Cernicharo. Gahm et al. found that many objects had radii under 10,000 AU, with a distribution peak around 25,000 AU. The distribution of mass for the globulettes above a detection limit of  $1 M_J$  peaked at about  $13 M_J$ , with only a few objects exceeding  $60 M_J$ . No near-infrared counterparts have been found to be convincingly associated with the globulettes, possibly indicating that none of these objects is a genuine proplyd or a protostar. Virial analysis yields the result that above 60% of the globulettes have conditions for gravitational contraction. Furthermore, the free-fall times were estimated to be of a few times  $10^5 \text{ yr}$ , or about one order of magnitude shorter than the photoevaporation times, estimated to be of the order of 3 to 4 Myr. This large photoevaporation timescale is surprisingly large in the harsh environment of NGC 2244, but may be due to a process of slow compression that follows the erosion of the outer layers by photoevaporation. One of the most interesting conclusions from this study is that the small Rosette Nebula globules may be the predecessors to brown dwarfs or planetary mass objects, reinforcing the idea that these kind of low mass objects can form in isolation following a process of contraction similar to stars, and not only by ejection or disruption of protoplanetary disks.

## 5. Final Remarks

After 80 years of studies, the Rosette Complex is known as one of the most important astrophysical laboratories for the study of the many aspects of star formation.

A solid basis for the investigation of the Rosette Complex has been successfully set. We have now a very detailed picture of the physical properties of the HII region and the molecular cloud, and we have located the majority of the stars that have formed across the complex. The Rosette has been actively forming stars for the last 2 to 3 Myr (based on the age of NGC 2244) and it will probably continue doing so, as there is still sufficient molecular material ( $> 1 \times 10^5 M_{\odot}$ ), placed in a heavily stimulated environment: The large photodissociation region excavated by the OB association NGC 2244 is in clear interaction with the adjacent molecular cloud, which after several years of investigations has revealed an abundant embedded population. Also, it appears that another population of young, low mass stars could form in the surroundings of the central

cavity (NGC 2237, REFL10 and the small globules, if they are truly predecessors to low mass objects). Could these be evidence of triggered formation?

The formation of embedded clusters and associations in the adjacent molecular cloud was clearly affected by the interaction with the nebula, but we still have to understand the extent of that interaction. The different cluster formation episodes appear to suggest that the current star forming properties of the Rosette Molecular Cloud could be related to the early evolution of the cloud, and not only to the interaction with the HII region.

In the near future it will be necessary to investigate the possible differences in the mechanisms of cluster formation, the variations in the star formation efficiency across the cloud, the observed properties of clusters and the definitive role of the local environment. All of this information will be of enormous value for the global study of star formation.

Now that the second generation of clusters in the Rosette has been identified, it is expected to be studied in even greater detail using infrared spectroscopy. Such investigations will be of great help to constrain the relative ages of the embedded populations and to reconstruct the history of formation in the region. Also, the near-future development of observational technologies and continuous improvements in the modeling of the interstellar medium and formation of clusters are promising, to say the least, for one of the most notorious targets in modern astronomy.

**Acknowledgment.** We would like to thank Jonathan Williams for insightful comments during the preparation of this chapter and Joanna Levine for editing an early version of the manuscript. We greatly acknowledge the referee Leo Blitz and the editor Bo Reipurth for providing corrections that vastly improved the chapter text. We also thank Harvey Liszt, Leisa Townsley, Jonathan Williams, Robert Gendler, and Ignacio de la Cueva Torregrosa for generously sharing images which we used in some of the figures.

Carlos Román-Zúñiga wants to acknowledge CONACYT, Mexico for a fellowship that sponsored his doctoral studies at the University of Florida.

Elizabeth Lada acknowledges support from the NASA grant NNG05D66G issued through the LTSA program to the University of Florida. Data obtained with the instrument FLAMINGOS and presented in this work were collected under the NOAO Survey Program, "Towards a Complete Near-Infrared Spectroscopic Survey of Giant Molecular Clouds" (PI: E. Lada) which is supported by NSF grants AST97-3367 and AST02-02976 to the University of Florida. FLAMINGOS was designed and constructed by the IR instrumentation group (PI: R. Elston) at the University of Florida, Department of Astronomy, with support from NSF grant AST97-31180 and Kitt Peak National Observatory.

This publication makes use of data products from the Two Micron All Sky Survey, which is a joint project of the University of Massachusetts and the Infrared Processing and Analysis Center/California Institute of Technology, funded by the National Aeronautics and Space Administration and the National Science Foundation.

## References

- Aharonian, F. A., Akhperjanian, A. G., Beilicke, M. et al. 2004, *A&A*, 417, 973  
 Aharonian, F. A., Akhperjanian, A. G., Bazer-Bachi, A. R. et al. 2007, *A&A*, 469, L1  
 Aspin, C. 1998, *A&A*, 335, 1040

- Bagnulo, S., Hensberge, H., Landstreet, J. D., Szeifert, T., & Wade, G. A. 2004, *A&A*, 416, 1149
- Balog, Z., Muzerolle, J., Rieke, G. H., Su, K. Y. L., Young, E. T., & Megeath, S. T. 2007, *ApJ*, 660, 1532
- Barnard, E. E. 1894, *Astronomy and Astrophysics*, 13, 642
- Berghöfer, T. W. & Christian, D. J. 2002, *A&A*, 383, 890
- Blitz, L. 1993 in *Protostars and Planets III*, eds. E. H. Levy & J. I. Lunine, Univ. of Arizona Press, p. 125
- Blitz, L., & Stark, A. A. 1986, *ApJ*, 300, L89
- Blitz, L., & Thaddeus, P. 1980, 241, 676
- Block, D. 1990, *Nat*, 347, 452
- Block, D., Dyson, J. E., & Madsen, C. 1992, *ApJ*, 390, L13
- Carlqvist, P., Kristen, H., & Gahm, G. F. 1998, *A&A*, 332, L5
- Carlqvist, P., Gahm, G. F., & Kristen, H. 2002, *Ap&SS*, 280, 405
- Carpenter, J. M. 2000, *AJ*, 120, 3139
- Celnik, W. E. 1983, *A&AS*, 53, 403
- Celnik, W. E. 1985, *A&A*, 144, 171
- Celnik, W. E. 1986, *A&A*, 160, 287
- Chen, W. P., Chiang, P. S., & Li, J. Z. 2004, *ChJAA* Vol. 4, 2, 153
- Clayton, C. A. & Meaburn, J. 1995, *A&A*, 302, 202
- Clayton, C. A., Meaburn, J., López, J. A., Christopoulou, P. E., & Goudis, C. D. 1998, *A&A*, 334, 264
- Cohen, M. 1973, *ApJ*, 185, L75
- Cox, P. 1989, *A&A*, 225, L1
- Cox, P., Deharveng, L., & Leene, A. 1990, *A&A*, 230, 181
- D'Antona, F., & Mazzitelli, I. 1997 in *Cool stars in Clusters and Associations*, eds. R. Pallavicini & G. Micela, *Mem.S.A.It.*, 68, n.4
- Davies, R. D. 1963, *Observatory*, 83, 172
- Davies, R. D., Elliott, K. H., Goudis, C., Meaburn, J., & Tebbutt, N. J. 1978, *A&AS*, 31, 271
- Deshpande, A. A., Shevgaonkar, R. K., & Sastry, Ch. V. 1984, *Ap&SS*, 102, 21
- Elmegreen, B. G. & Lada, C. J. 1977 *ApJ*, 214, 725
- Feigelson, E. D., Getman, K., Townsley, L. Garmire, G., Preibisch, T., Grosso, N., Montmerle, T., Muench, A. & McCaughrean, M. 2005, *ApJS*, 160, 379
- Flynn, F. H. 1965, *MNRAS*, 130, 9
- Fountain, W. F., Gary, G. A., & O'Dell, C. R. 1979, *ApJ*, 229, 971
- Gahm, G. F., Grenman, T., Fredriksson, S., & Kristen, H. 2007, *AJ*, 133, 1795
- Gonzalez-Alfonso, E., & Cernicharo, J. 1994, *ApJ*, 430, L125
- Gosachinskii, I. V. & Khersonskii, V. K. 1982, *Soviet Astronomy*, 26, 146
- Graham, D. A., Haslam, C. G. T., & Wilson, W. E. 1982, *A&A*, 109, 145
- Gregorio-Hetem, J., Montmerle, T., Casanova, S., & Feigelson, E. D. 1998, *A&A*, 331, 193
- Guseva, N. G., Kolesnik, I. G., & Kravchuk, S. G. 1984, *Soviet Astronomy Letters*, 10, 309
- Haisch, K. E., Jr., Lada, E. A., & Lada, C. J. 2001, *ApJ*, 553, L153
- Harvey, P. M., Campbell, M. F., & Hoffmann, W. F. 1977, *ApJ*, 215, 151
- Hensberge, H., Vrancken M., & Verschueren W. 1998, *A&A*, 339, 141
- Hensberge, H., Pavlovsky, K., & Verschueren, W. 2000, *A&A*, 358, 553
- Héraudeau, P., Simien, F., & Mamon, G. A. 1996, *A&A*, 117, 417
- Herbig, G. H. 1974, *PASP*, 86, 604
- Herschel, J. 1864, *Phil. Trans. Roy. Soc. Lon.*, 154, 1
- Heyer, M. H. & Schloerb, F. P. 1997, *ApJ*, 475, 173
- Heyer, M. H., Williams, J. P., & Brunt, C. M. 2006, *ApJ*, 643, 956
- Hjellming, R. M. 1968, *ApJ*, 154, 533
- Holdaway, M., Braun R., & Liszt H. S. 1999 (unpublished)
- Howells, L., Steele, I. A., Porter, J. M., & Etherton, J. 2001, *A&A*, 369, 99
- Hubble, E. P. 1922, *ApJ*, 56, 400
- Ishii, M., Hirao, T., Nagashima, C., Nagata, T., Sato, S., & Yao, Y. 2002, *AJ*, 124, 430

- Jaffe, T. R., Bhattacharya, D., Dixon, D. D., & Zych, A. D. 1997, *AJ*, 484, L129
- Johnson, H. L. 1962, *ApJ*, 136, 1135
- Kahn, F. D. & Menon, T. K. 1961, *Proceedings of the National Academy of Sciences*, 47, 1712
- Kaidanovskii, M. N. 1980, *Soviet Astronomy*, 24, 201
- Kirillova, T. S. 1958, *Trudy Gosudarstvennogo Astronomicheskogo Instituta*, 29, 178
- Ko, H. C. & Kraus, J. D. 1955, *Nat*, 176, 221
- Krymkin, V. V. 1978, *Ap&SS*, 54, 187
- Kuchar T. A. & Bania, T. M. 1993, *ApJ*, 414, 664
- Lada, C. J. & Gautier, T. N. 1982, *ApJ*, 261, 161
- Lada, C.J. & Lada, E.A. 2003, *ARA&A*, 41, 57
- Lada, E. A., DePoy, D. L., Evans, N. J., & Gatley, I. 1991, *ApJ*, 371, 171
- Lasker, B. M. 1966, *ApJ*, 143, 700
- Lassell, W. 1867, *MmRAS*, 36, 53
- Leahy, D. A. 1985, *MNRAS*, 217, 69
- Leahy, D. A., Naranan, S., & Singh, K. P. 1986, *MNRAS*, 220, 501
- Li, J. Z., Wu, C. H., Chen, W. P., Rector, T., Chu, Y. H., & Ip, W. H. 2002, *AJ*, 123, 2590
- Li, J. Z. 2003, *ChJAA Lett.*, 6, 495
- Li, J. Z. 2005, *ApJ*, 625, 242
- Li, J. Z. & Rector T. A. 2004, *ApJ*, 600, L67
- Li, J. Z. & Rector T. A. 2007, *New Astronomy*, 12, 441
- Li, J. Z. & Smith, M. D. 2005, *ApJ*, 620, 816
- Li, J. Z., Chu, Y., Gruendl, R., Bally, J. & Su, W. 2007, *ApJ*, 659, 1373
- Loren, R. B. 1981, *ApJ*, 245, 495
- Maddalena, R. J. & Thaddeus, P. 1985, *ApJ*, 294, 231
- Marschall, L. A., van Altena, W. F., & Chiu, L. G. 1982, *AJ*, 87, 1497
- Massey, P., Johnson, K. E., & DeGioia-Eastwood, K. 1995, *ApJ*, 454, 151
- Mathews, W. G. 1966, *ApJ*, 144, 206
- Mathews, W. G. 1967, *ApJ*, 147, 965
- Meaburn, J., López, J. A., Richer, M. G., & Riesgo H. 2005, *AJ*, 130, 730
- Meaburn, J. & Walsh, J. R. 1986, *MNRAS*, 220, 745
- Menon, T. K. 1962, *ApJ*, 135, 394
- Meyer, M. R., Calvet, N., & Hillenbrand, L. 1997, *AJ*, 108, 1382
- Minkowski, R. 1949, *PASP*, 61, 361
- Odegard, N. 1986, *ApJ*, 301, 813
- Ogura, K. & Ishida, K. 1981, *PASJ*, 33, 149
- Park, B. & Sung, H. 2002, *AJ*, 123, 892
- Patel, N. A., Xie, T., & Goldsmith, P. F. 1993, *ApJ*, 413, 593
- Pedlar, A. & Matthews, H. E. 1973, *MNRAS*, 165, 381
- Phelps R. L. & Lada, E. A. 1997, *ApJ*, 477, 176
- Phelps, R. L. & Ybarra, J. E. 2005, *ApJ*, 627, 845
- Pérez, M. R., Thé, P. S., & Westerlund, B. E. 1987, *PASP*, 99, 1050
- Pérez, M. R., Joner, M. D., Thé, P. S., & Westerlund, B. E. 1989, *PASP*, 101, 195
- Poulton, C. J., Robitaille, T. P., Greaves, J. S., Bonnell, I. A., Williams, J. P. & Heyer, M. H. 2008, *MNRAS*, 384, 1249
- Román-Zúñiga, C. G. 2006, Ph.D. thesis, University of Florida
- Román-Zúñiga, C. G., Elston, R., Ferreira, B. & Lada, E. A., 2008, *ApJ*, 672, 861
- ROSAT Consortium 2000, *ROSAT Newsl.*, 71
- Scalo, J. M. 1986, *Fundamentals of Cosmic Physics*, 11, 1
- Shipman, R. F. & Clark, F. O. 1994, *ApJ*, 422, 153
- Shipman, R. F. & Carey, S. J. 1996, *ApJ*, 469, L131
- Schneider, N., Stutzki, J., Winnewisser, G., & Block, D. 1998a, *A&A*, 335, 1049
- Schneider, N., Stutzki, J., Winnewisser, G., Poglitsch, A. and Madden, S. 1998b, *A&A*, 338, 262
- Schneps, M. H., Ho, P. T. P., & Barrett, A. H. 1980, *ApJ*, 240, 84
- Smith, M. G. 1968, *Ap&SS*, 1, 68

- Smith, M. G. 1973, ApJ, 182, 111  
Subramaniam, A., Sahu, D. K., Sagar, R., & Vijitha, P. 2005, A&A, 440, 511  
Sugitani, K., Fukui, Y., & Ogura, K. 1991, ApJS, 77, 59  
Swift, L. 1886, Astronomische Nachrichten 113 (catalogue 2707)  
Tsivilev, A. P., Poppi, S., Cortiglioni, S., Palumbo, G. G. C., Orsini, M., & Maccaferri, G. 2002, New Astronomy, 7, 449.  
Townsley, L. K., Feigelson, E. D., Montmerle, T., Broos, P. S., Chu, Y., & Garmire, G. P. 2003, ApJ, 593, 874  
Turner, D. G. 1976, ApJ, 210, 65  
Verschueren, W. 1991, Ph.D. thesis, Vrije Univ. Brussels.  
Viner, M. R., Vallée, J. P., & Hughes, V. A. 1979, AJ, 84, 9  
Wang, J., Townsley, L. K., Feigelson, E. D., Broos, P., Getman, K., Román-Zúñiga, C. G. & Lada, E. A. 2008, ApJ, 675, 464  
White, G. J., Lefloch, B., Fridlund, C. V. M., Aspin, C., Dahmen, G. et al. 1997, A&A, 323, 931  
Williams, J., de Geus E. J., & Blitz, L. 1994, ApJ, 428, 693  
Williams, J. P., Blitz, L., & Stark, A. A. 1995, ApJ, 451, 252  
Ybarra, J. E. & Phelps, R. L. 2004, AJ, 127, 3444